

EIGENMODE ANALYSIS OF GALAXY DISTRIBUTIONS IN REDSHIFT SPACE

TAKAHIKO MATSUBARA

Department of Physics and Astrophysics, Nagoya University, Chikusa, Nagoya 464-8602, Japan

ALEXANDER S. SZALAY, ADRIAN C. POPE

Department of Physics and Astronomy, The Johns Hopkins University, Baltimore, MD 21218

Draft version October 29, 2018

ABSTRACT

Eigenmode analysis is one of the most promising methods of analyzing large data sets in ongoing and near-future galaxy surveys. In such analyses, a fast evaluation of the correlation matrix in arbitrary cosmological models is crucial. The observational effects, including peculiar velocity distortions in redshift space, light-cone effects, selection effects, and effects of the complex shape of the survey geometry, should be taken into account in the analysis. In the framework of the linear theory of gravitational instability, we provide the methodology to quickly compute the correlation matrix. Our methods are not restricted to shallow redshift surveys, arbitrarily deep samples can be dealt with as well. Therefore, our methods are useful in constraining the geometry of the universe and the dark energy component, as well as the power spectrum of galaxies, since ongoing and near-future galaxy surveys probe the universe at intermediate to deep redshifts, $z \sim 0.2$ –5. In addition to the detailed methods to compute the correlation matrix in 3-dimensional redshift surveys, methods to calculate the matrix in 2-dimensional projected samples are also provided. Prospects of applying our methods to likelihood estimation of the cosmological parameters are discussed.

Subject headings: cosmology: theory — galaxies: distances and redshifts — galaxy clustering — large-scale structure of universe — methods: statistical

1. INTRODUCTION

The large-scale structure (LSS) of the universe offers invaluable information on cosmology. The clustering pattern of galaxies reflects what the primordial universe looks like and how the universe evolves. In contrast to the observations of the cosmic microwave background (CMB), in which only information from photons emitted at a fixed redshift $z_{\text{dec}} \simeq 1090$ are observed, the observations of the LSS provide information from photons emitted at various redshifts $z \lesssim 5$. Therefore, while the CMB primarily tells us the state of the early universe, the LSS shows us that of the present universe and its recent evolution. Detailed analysis of the LSS is extremely important in order to obtain a consistent picture of the evolving universe.

The spatial distribution of galaxies has particular importance in cosmology. Traditionally the power spectrum, or the correlation function is computed from galaxy distributions and is compared with theoretical predictions. Strictly speaking, the power spectrum and the correlation function are properly evaluated only when the sample is homogeneous. In a real-world observation, homogeneous sampling of galaxies is not possible. The sampling density varies with radial distance, and possibly with survey directions. The survey geometry may have a complex shape. The observed galaxies are inevitably on a light-cone, therefore evolutionary effect comes in when a survey has a certain depth.

Therefore, estimating the power spectrum from a real data needs a method to approximately erase those sources of inhomogeneity. Among others, Feldman, Kaiser, & Peacock (1994) offers a standard method to estimate the power spectrum. The estimated power spectrum by such standard method is a convolution of the true power with the window function of the survey. This becomes a problem when the survey has a complex shape.

In a seminal paper, Vogeley & Szalay (1996) introduced a novel method, i.e., the method of Karhunen-Loève (KL) eigenmodes in the context of galaxy redshift surveys. This method can handle complex shape of the survey geometry as well as complex selection functions. In the context of CMB analysis, Bond (1995) introduced an equivalent method which is called signal-to-noise eigenmodes method. The KL method is now recognized as one of the most promising methods to tackle large data sets of the cosmological surveys (Tegmark, Taylor, & Heavens 1997; Tegmark et al. 1998; Taylor, Ballinger, Heavens, & Tadros 2001), and has been successfully applied to the Las Campanas Redshift Survey (LCRS) (Matsubara, Szalay & Landy 2000), the Sloan Digital Sky Survey (SDSS) (Szalay et al. 2003; Pope et al. 2004), the ROSAT-ESO Flux-Limited X-Ray (REFLEX) Galaxy Cluster Survey (Schuecker, Guzzo, Collins, & Böhringer 2002). A variant, simplified method, which is called pseudo-KL eigenmodes method is applied to the IRAS Point Source Catalog Redshift Survey (PSCz) (Hamilton, Tegmark, & Padmanabhan 2000), the 2dF Galaxy Redshift Survey (Tegmark, Hamilton, & Xu 2002), and SDSS (Tegmark et al. 2003).

In applying the KL technique to cosmology, it is important to have a good method to theoretically compute the power spectrum of the KL modes. This is not a trivial task, since the observed distribution of the galaxies are distorted by observational effects including peculiar velocity distortions, light-cone effects, varying selection functions, and complex shape of the survey geometry. Among these, the light-cone effect has never been taken into account in previous applications of the KL method to redshift surveys. The light-cone effects consist of evolutionary effects and geometric effects. The

clustering of galaxies evolves with redshift through evolution in mass clustering, and evolution in the biasing of galaxies. The comoving distance is not proportional to the redshift and the apparent clustering pattern in redshift space is not the same as in comoving space. For shallow redshift surveys in which the redshift range is, e.g., $0 \lesssim z \lesssim 0.2$, the light-cone effect has small contributions. However, QSO surveys probe much deeper regions, and ongoing and near-future redshift surveys, like the Deep Extragalactic Evolutionary Probe (DEEP) survey (e.g., Davis et al. 2003), the SDSS Luminous Red Galaxy (LRG) survey (Eisenstein et al. 2001), and the Kilo-Aperture Optical Spectrograph (KAOS) project¹ probe the universe of redshifts $0.2 \lesssim z \lesssim 5$.

Therefore, it is crucial in cosmological analyses of large surveys to have a good methodology in applying the KL eigenmodes method to ongoing and near-future redshift surveys which are not necessarily shallow. In this paper, methods to efficiently evaluate the theoretical values of the correlation matrix, playing a central role in the KL analysis, are developed and described in detail. This paper is organized as follows. In §2 the Bayesian analysis of the large data set in the context of galaxy surveys is reviewed, and necessity of a fast method to compute the correlation matrix is explained. In §3 the central method of this paper is presented. Necessary quantities in describing the method are introduced in §3.1. A fast method to compute the linear correlation matrix in redshift space is given in §3.2 and §3.3. The nonlinear Finger-of-God effect is discussed in §3.4. Fast methods to compute the linear correlation matrix in projected 2-dimensional samples are provided in §3.5. In §4 additional techniques in applying the present methods to the KL eigenmodes are explained. Finally, the presented methods are summarized and discussed in §5.

2. THE EIGENMODE ANALYSIS AND IMPORTANCE OF THE CORRELATION MATRIX

In this section we briefly review the eigenmode analysis originally introduced by Vogeley & Szalay (1996) in the context of the redshift surveys. The importance of accurately modeling the correlation matrix in redshift space and of developing a numerically fast algorithm to calculate the model matrices, which are the main subject of this work, will be clarified in this section.

2.1. Bayesian Analyses of the Huge Data Sets

One of the central motivation of the eigenmode analysis comes from the difficulty in direct Bayesian analysis of huge data sets of observed galaxy distributions. It is desirable that the cosmological models are discriminated by the galaxy distribution itself, not relying on the inverse problem of determining the underlying density power spectrum from observed galaxy distributions. While a cosmological model predicts the linear power spectrum, the dependence of the galaxy clustering in redshift surveys on the theoretical power spectrum is not simple.

Nonlinearity in the gravitational evolution distorts the power spectrum on small scales $\lesssim 10 h^{-1}\text{Mpc}$. Peculiar velocities anisotropically distort the power spectrum on all scales. Spatial variation of the mass-to-light ratio or the galaxy biasing distorts the power spectrum. In deep redshift surveys, the spatial curvature and the evolution of the Hubble parameter distort the apparent pattern of the galaxy clustering. These various distortions in the observed power spectrum also depend on the cosmological model. Even if one can invent and adopt some ansatz on such a complex inversion problem, fair amount of information will be lost in this inversion process.

However, the reconstruction of the underlying power spectrum is not necessary to discriminate the cosmological models. In the Bayesian approach, the posterior probability of the set of model parameters $\Theta = \{\theta_\alpha\}$, given a set of observational data $D = \{d_i\}$ and additional prior information I , is estimated by Bayes's theorem:

$$P(\Theta|D, I) = P(\Theta|I) \frac{P(D|\Theta, I)}{P(D|I)}. \quad (2.1)$$

The first factor is the Bayesian prior, i.e., the prior knowledge on the model parameters, and the denominator is the normalization constant. Evaluating the numerator is the crucial part of the Bayesian approach. One needs to repeatedly evaluate this factor to maximize the posterior probability in multi-dimensional parameter space. Therefore, the numerator should be numerically calculated as fast as possible. This part of the calculation is usually not easy, especially when the data D consists of a large set of observational figures. In galaxy redshift surveys, the data D consists of the distribution of galaxies in redshift space. These days the scales of redshift surveys become more and more immense. In the 2dF Galaxy Redshift Survey (Colless et al. 2001), redshifts of about 220,000 galaxies are observed in the sky coverage of 2,000 square degrees. In the Sloan Digital Sky Survey (SDSS) (York et al. 2000), redshifts of about 1,000,000 galaxies are planned to be observed over 10,000 square degrees of the sky.

When the prior information on the model, I , has nothing to do with obtaining the data themselves, the numerator of equation (2.1) is equal to $P(D|\Theta)$. In addition, when the statistical distribution of the data D is given by the multivariate Gaussian distribution, this factor has the form,

$$P(D|\Theta) = \frac{1}{\sqrt{(2\pi)^N \det R(\Theta)}} \exp \left[-\frac{1}{2} \left(\mathbf{d}^T - \langle \mathbf{d}^T \rangle_\Theta \right) R^{-1}(\Theta) (\mathbf{d} - \langle \mathbf{d} \rangle_\Theta) \right], \quad (2.2)$$

where \mathbf{d} is the data vector $\mathbf{d} = (d_1, d_2, \dots, d_N)^T$ and R is the $N \times N$ correlation matrix given by

$$R(\Theta) = \left\langle (\mathbf{d} - \langle \mathbf{d} \rangle_\Theta) (\mathbf{d} - \langle \mathbf{d} \rangle_\Theta)^T \right\rangle_\Theta = \left\langle \mathbf{d} \mathbf{d}^T \right\rangle_\Theta - \langle \mathbf{d} \rangle_\Theta \langle \mathbf{d}^T \rangle_\Theta. \quad (2.3)$$

¹ <http://www.noao.edu/kaos/>

In the above notations, $\langle \cdots \rangle_\Theta$ indicates the ensemble average over the statistical realizations of the universe (see, e.g., Peebles 1980) for an assumed set of model parameters Θ . The correlation matrix therefore explicitly depends on the model parameters.

In the analysis of redshift surveys, the observed set of data is primarily a set of the positions of galaxies in redshift space. The density field is derived from this primary data, which is one of the most fundamental information of our universe in redshift surveys. Therefore, it is natural that the data D is identified as the number density field of galaxies in redshift space. For this purpose, the redshift space is pixelized to obtain a discretized set of galaxy counts. Thus, the set of the number counts d_i in a cell i is the data D in redshift surveys. The pixel size determines the resolution in the analysis, so it is desirable to adopt as many cells in redshift space as possible. However, too many cells cause trouble in calculating the inverse of the correlation matrix in equation (2.2). The calculation of the inverse of the huge matrix requires a lot of computation time, which is primarily an N^3 process and can be an $N^{2.8}$ process at most (Press et al. 1992). This is the bottle neck in the Bayesian analysis since the inversion should be repeatedly performed for every set of parameters.

The pixelized raw data vector $\mathbf{d} = (d_1, d_2, \dots, d_N)^T$ consists of clustering signals and noises. Most of the process in inverting the correlation matrix in the above procedure might be devoted to dealing with noises. Since the information on the cosmological model is only contained in the signals, it is beneficial to reduce the dimension of the correlation matrix, keeping the maximal information on the clustering signals and minimizing contributions by the noise. One simple way to achieve this aim is to consider a linear projection of the raw data vector \mathbf{d} into vector \mathbf{B} of a smaller dimension:

$$\mathbf{B} = P\mathbf{d}, \quad (2.4)$$

where the projection matrix P has a dimension $M \times N$, and the dimension of the vector \mathbf{B} is M , where $M < N$. The correlation matrix of the reduced data vector is given by

$$C(\Theta) = \left\langle (\mathbf{B} - \langle \mathbf{B} \rangle_\Theta) (\mathbf{B} - \langle \mathbf{B} \rangle_\Theta)^T \right\rangle_\Theta = PR(\Theta)P^T. \quad (2.5)$$

The linear transformation from \mathbf{d} to \mathbf{B} ensures the preservation of the Gaussianity of the distribution.

A clever choice of the projection matrix P enables us to avoid the inversion of the originally huge correlation matrices without losing most of the information contained in signals. In such a case, the inversion of smaller correlation matrices for the reduced data suffices for the Bayesian analysis, and the computation time is reduced by a factor of about $(M/N)^{2.8}$. In Appendix A, the construction of the projection matrix by the KL eigenmodes with maximal signal-to-noise ratio is comprehensively reviewed. In short, the projection matrix by KL eigenmodes picks the first M modes that have largest S/N ratio.

The probability of having a reduced data set, $D_{\text{reduced}} = \{B_n\}$, given the set of model parameters, Θ , is therefore given by

$$P(D_{\text{reduced}}|\Theta) = \frac{1}{\sqrt{(2\pi)^M \det C(\Theta)}} \exp \left[-\frac{1}{2} \left(\mathbf{B}^T - \langle \mathbf{B}^T \rangle_\Theta \right) C^{-1}(\Theta) (\mathbf{B} - \langle \mathbf{B} \rangle_\Theta) \right]. \quad (2.6)$$

The above equation assumes that the procedure of obtaining data is independent of the assumed model parameters, so that the projection matrix should be fixed throughout analyzing and maximizing the likelihood function. However, the optimal choice of the projection matrix usually depends on the underlying correlation function, and thus on model parameters, as explicitly presented in Appendix A in the case of the KL-mode projection. Therefore, the projection matrix is initially constructed by a fiducial set of model parameters, which is fixed throughout the maximization of the likelihood function.

While the reduced correlation matrix C constructed by KL eigenmodes is diagonalized for a fiducial set of model parameters, it should be noted that the correlation matrix C is *not* diagonal for other set of model parameters. Therefore, the inversion of the correlation matrix C still needs to be performed. The likelihood function is not biased by the initial choice of the fiducial model, because the fiducial parameters only determine the projection matrix P which is fixed throughout. If the initial choice of the fiducial model is far from the correct model, the projection matrix is not the optimal one, and therefore we obtain rather broader profile of the likelihood function around the maximum, because of picking low-S/N modes. One can iterate the likelihood maximization by choosing a fiducial model from the preceding estimation to acquire the narrower profile of the likelihood function. This is the procedure we apply in practical situations.

The model correlation matrix $C(\Theta)$ of a reduced data set should be repeatedly calculated for various models, fixing the projection matrix P . One still needs to construct the $N \times N$ matrix $R(\Theta)$ as many times as C , because $C(\Theta) = PR(\Theta)P^T$. It is only when this process is omitted that the parameter dependence on R is linear or polynomial. However, most of the important parameters are not linearly or polynomially dependent on the correlation matrix. On that ground, a good modeling and numerically fast construction of the correlation matrix R is essential.

2.2. Bayesian Analysis of the Galaxy Distribution in Redshift Surveys

Now we turn our attention to the application of the general method explained above to the analysis of the data in galaxy redshift surveys. The primary data set in redshift surveys is the galaxy distribution in redshift space. In order to directly deal with the galaxy distribution, first we pixelize the redshift space, and then build the data vector \mathbf{d} from galaxy counts d_i in cells of the volume V_i . The expected counts $N_i = \langle d_i \rangle$ are given by an integral of the selection function $n(\mathbf{s})$, i.e., expected number density field in a survey:

$$N_i = \int d^3s K_i(\mathbf{s}) n(\mathbf{s}), \quad (2.7)$$

where $K_i(\mathbf{s})$ is the kernel function of a cell i , which is centered at \mathbf{s}_i , and normalized by $\int d^3s K_i(\mathbf{s}) = V_i$. For example, the top-hat kernel of smoothing radius R is given by $K_i(\mathbf{s}) = \Theta(R - |\mathbf{s} - \mathbf{s}_i|)$ and $V_i = 4\pi R^3/3$, where $\Theta(x)$ is the Heaviside step function and \mathbf{s}_i is the center of the cell i . We require the knowledge of the selection function in a survey. The correlation matrix is given by the moments of the count-in-cells (Peebles 1980), and is related to the convolution of the two-point correlation function in redshift space, $\xi^{(s)}(\mathbf{s}, \mathbf{s}')$. Including the shot noise term, the relation is

$$R_{ij} = \int d^3s d^3s' K_i(\mathbf{s}) K_j(\mathbf{s}') n(\mathbf{s}) n(\mathbf{s}') \xi^{(s)}(\mathbf{s}, \mathbf{s}') + \int d^3s K_i(\mathbf{s}) K_j(\mathbf{s}) n(\mathbf{s}) + E_{ij}, \quad (2.8)$$

where the first term corresponds to the signal, second term corresponds to the shot noise, and the last term, E_{ij} , is the correlation matrix for other sources of noise such as magnitude errors or uncertainty in the luminosity function, which is assumed to be independent from the clustering signal for simplicity. One can reasonably assume that the selection function $n(\mathbf{s})$ within each cell is approximately constant and can be replaced by $n_i = N_i/V_i$, in which case the equation (2.8) reduces to

$$R_{ij} = N_i N_j \xi_{ij}^{(s)} + \sqrt{N_i N_j} K_{ij} + E_{ij}, \quad (2.9)$$

(no sum over i, j) where

$$\xi_{ij}^{(s)} = \frac{1}{V_i V_j} \int d^3s d^3s' K_i(\mathbf{s}) K_j(\mathbf{s}') \xi^{(s)}(\mathbf{s}, \mathbf{s}'), \quad (2.10)$$

and

$$K_{ij} = \frac{1}{\sqrt{V_i V_j}} \int d^3s K_i(\mathbf{s}) K_j(\mathbf{s}). \quad (2.11)$$

The first term in equation (2.9) contains the model parameters, and corresponds to the signal part of the correlation matrix, S_{ij} . The second term corresponds to the shot noise. When the cells do not overlap, the matrix K_{ij} is diagonal:

$$K_{ij} = \frac{\delta_{ij}}{V_i} \int d^3s K_i^2(\mathbf{s}), \quad (\text{non-overlapping}), \quad (2.12)$$

(no sum over i, j), where δ_{ij} is the Kronecker's delta. For the non-overlapping top-hat kernel, this equation is simplified as $K_{ij} = \delta_{ij}$, and the correlation matrix is simply given by

$$R_{ij} = N_i N_j \xi_{ij}^{(s)} + N_i \delta_{ij} + E_{ij}, \quad (\text{non-overlapping, top-hat}) \quad (2.13)$$

(no sum over i, j).

Unlike the correlation function in real space, the correlation function in redshift space is neither isotropic nor homogeneous. The correlation function in real space is a function of separations between two-points, $\xi(|\mathbf{x}_1 - \mathbf{x}_2|)$. However, the redshift space is distorted from the real space, and consequently the correlation function is no longer the function of the separation only.

The comoving distance to a galaxy is not a primary observable quantity and the redshift is the only estimate of the real distance from the Earth to the cosmologically distant galaxies. Since the redshift is not identical to the comoving distance, the redshift space is anisotropically distorted from the real space. There are two predominant sources for the redshift-space distortion.

The first source of the distortion is the peculiar velocities of galaxies. The peculiar velocities along the line of sight increase or decrease the observed redshift by the Doppler effect. On nonlinear scales, the peculiar velocities are dominated by the random motion in a cluster potential. On linear scales, the coherent motion along the density gradient is predominant. The linear velocity distortions are relatively simple when the distant-observer (or plane-parallel) approximation is applied. Kaiser (1987) found the linear power spectrum in redshift space, $P^{(s)}(\mathbf{k})$ is anisotropically distorted along the line of sight, and is given by the formula,

$$P^{(s)}(\mathbf{k}) = (1 + \beta \mu_{\mathbf{k}}^2)^2 P(k), \quad (2.14)$$

where $P(k)$ is the power spectrum in real space, $\mu_{\mathbf{k}}$ is the cosine of the wavevector \mathbf{k} to the line of sight. The counterpart of this formula for the linear two-point correlation function, $\xi^{(s)}(\mathbf{r})$, which is given by the Fourier transform of equation (2.14), was derived by Hamilton (1992).

The second source of the distortion is what is called Alcock-Paczyński (AP, hereafter) effect. Alcock & Paczyński (1979) pointed out that the spherical objects in deep redshift region appears to be distorted in redshift space because of the nonlinear relation between the redshift and the comoving distance, and of the nonlinear relation between the apparent angular size and the angular diameter distance. Suppose that there is a spherical object of diameter l in units of comoving length. The redshift difference of this object is $\Delta z = H(z)l/c$, and the apparent angular size is $\Delta\theta = l/D_A(z)$, where $H(z)$ is the redshift-dependent Hubble parameter and $D_A(z)$ is the comoving angular diameter distance [proper angular diameter distance is given by $d_A(z) = D_A(z)/(1+z)$]. The ratio

$$\frac{\Delta z}{z \Delta\theta} = \frac{D_A(z)}{cz/H(z)} \quad (2.15)$$

is unity for sufficiently small z . In deep redshift regions, however, the ratio significantly deviates from unity and the deviation pattern strongly depends on the density parameter Ω_{M0} and on the cosmological constant $\Omega_{\Lambda 0}$, or parameters of the dark energy.

The redshift-space distortions of the two kinds, i.e., the velocity distortions and the AP distortions, are interwoven in the real universe except for the shallow redshift surveys without the AP effect. Ballinger, Peacock & Heavens (1996) derived the AP effect on the linear power spectrum, and Matsubara & Suto (1996) derived the same effect on the linear two-point correlation function, both using the distant observer approximation. Modern redshift surveys have survey geometries with wide opening angles. In these cases, the distant-observer approximation is inappropriate and the wide-angle effect is not negligible in order to handle the information contained in the survey. Szalay, Matsubara & Landy (1998) derived a formula of velocity distortions in the linear two-point correlation function with wide-angle effect. Matsubara (2000) derived the most general formula of the linear two-point correlation function in which the velocity distortions, the AP effect, and the wide-angle effect are all included in a unified formula. All the previous formulas for the linear two-point correlation function are limiting cases of the last formula. Our construction of the correlation matrix R , which is explained in the following section, takes full advantage of the last expression.

3. CONSTRUCTING CORRELATION MATRICES IN REDSHIFT SPACE

3.1. The General Formula of the Correlation Function in Redshift Space

To obtain the correlation matrix of equation (2.9), it is necessary to have the analytic expression of the correlation function $\xi^{(s)}(\mathbf{s}, \mathbf{s}')$, which is given by Matsubara (2000). For completeness, we reproduce the formula in this section. Before that, we need to introduce some basic notations.

The unperturbed metric is given by the Robertson-Walker (RW) metric,

$$ds^2 = -dt^2 + a^2(t) [dx^2 + S_K^2(x) (d\theta^2 + \sin^2 \theta \phi^2)], \quad (3.1)$$

where we employ the unit system with $c = 1$, and adopt a notation,

$$S_K(x) = \begin{cases} \frac{\sinh(\sqrt{-K}x)}{\sqrt{-K}}, & (K < 0), \\ x, & (K = 0), \\ \frac{\sin(\sqrt{K}x)}{\sqrt{K}}, & (K > 0), \end{cases} \quad (3.2)$$

The comoving angular diameter distance is related to the last function by

$$D_A(z) = S_K(x(z)). \quad (3.3)$$

where z is the “RW redshift” in which the peculiar velocity effect is not included, i.e., the redshift of the unperturbed universe. The radial coordinate x is the comoving distance from the observer, and the relation to the RW redshift is given by

$$x(z) = \int_0^z \frac{dz'}{H(z')}, \quad (3.4)$$

where $H(z) = \dot{a}/a$ is the time-dependent Hubble parameter. We consider the general case that the dark energy has an equation of state $p(z) = w(z)\rho(z)$, in which case,

$$H(z) = H_0 \sqrt{(1+z)^3 \Omega_{M0} - (1+z)^2 \Omega_{K0} + (1+z)^3 \exp\left(3 \int_0^z \frac{wdz}{1+z}\right) \Omega_{Q0}}, \quad (3.5)$$

where Ω_{M0} is the density parameter of matter(s), Ω_{Q0} is the density parameter of the dark energy, and $\Omega_{K0} = \Omega_{M0} + \Omega_{Q0} - 1$ is the curvature parameter.

The linear growth factor $D(z)$ is a growing solution of the ordinary differential equation,

$$\ddot{D} + 2H(z)\dot{D} - \frac{3}{2}H_0^2 \Omega_{M0}(1+z)^3 D = 0, \quad (3.6)$$

where the dot represents the differentiation with respect to the proper time t , and the proper time t is related to the RW redshift z by

$$t = \int_z^\infty \frac{dz'}{(1+z')H(z')}. \quad (3.7)$$

It is useful to transform the equation (3.6) to the following set of equations (Matsubara & Szalay 2003),

$$\frac{d \ln D}{d \ln a} = f, \quad (3.8)$$

$$\frac{df}{d \ln a} = -f^2 - \left(1 - \frac{\Omega_M}{2} - \frac{1+3w}{2} \Omega_Q\right) f + \frac{3}{2} \Omega_M, \quad (3.9)$$

where $a = (1+z)^{-1}$ is the scale factor of the universe, and

$$\Omega_M(z) = \frac{H_0^2}{H^2(z)} (1+z)^3 \Omega_{M0} \quad (3.10)$$

$$\Omega_Q(z) = \frac{H_0^2}{H^2(z)} \exp\left(3 \int_0^z \frac{1+w}{1+z} dz\right) \Omega_{Q0} \quad (3.11)$$

are the time-dependent density parameters of matter and dark energy, respectively. Determining both the growth factor, $D(z)$, and the logarithmic derivative of the growth factor, $f(z)$, is necessary in the formula of the redshift-space distortions. Accordingly, the Runge-Kutta integrations of the set of equations (3.8) and (3.9) meet the requirement.

The linear formula for the two-point correlation function in redshift space is presented in Appendix B. It has the form,

$$\xi^{(s)}(z_i, z_j, \theta_{ij}) = b_i b_j D_i D_j \sum_{n=0}^2 \sum_{l=0}^{2n} c_l^{(n)}(x_i, x_j, \theta_{ij}) \xi_l^{(n)}(x_{ij}), \quad (3.12)$$

where z_i and z_j are the redshifts of the two-points and θ_{ij} is the angle between them. The linear bias parameter $b(z)$ as a function of the redshift is introduced. The distances $x_i = x(z_i)$, $x_j = x(z_j)$ are comoving distances to the two points according to equation (3.4). The comoving separation x_{ij} between the two points is calculated by equation (B29). The functions $c_l^{(n)}$ are given by geometrical quantities and defined by equations (B30)–(B38). The functions $\xi_l^{(n)}$ are given by integrations of the power spectrum, and defined by equation (B27). Although the expression (3.12) is somewhat long, it is straightforwardly calculated once the single-variable functions $f(z)$, $D(z)$, $x(z)$, $b(z)$, $\xi_l^{(n)}(x)$ are calculated and tabulated beforehand for a fixed cosmological model.

While the correlation function linearly depends on the power spectrum through the function $\xi_l^{(n)}(x)$, the dependences on other cosmological parameters like Ω_{M0} , Ω_{Q0} , $w(z)$ are nonlinear. The bias parameter $b(z)$ only appears as 2nd order polynomials

3.2. Smoothing Integrations of the Correlation Function

Evaluating the correlation matrix of the equation (2.9) requires the six-dimensional integration of the correlation function in general. Direct integration is not a good idea. It is extremely important to obtain the elements of the correlation matrix without involving time-consuming steps such as multi-dimensional numerical integrations, because we need to construct many huge correlation matrices, with various cosmological models. We need to develop a method to calculate them with algebraic and interpolating methods without numerical integration for each element. There is actually such a method with special choices of the shape of the smoothing kernel as shown below.

The signal part of the correlation matrix of equation (2.10) is essentially the correlation function of the smoothed density contrast,

$$\xi_{ij}^{(s)} = \left\langle \delta_R^{(s)}(x_i, \theta_i, \phi_i) \delta_R^{(s)}(x_j, \theta_j, \phi_j) \right\rangle \quad (3.13)$$

where

$$\delta_R^{(s)}(x, \theta, \phi) = \int S_K^2(x') dx' \sin \theta' d\theta' d\phi' W_R(x, \theta, \phi; x', \theta', \phi') \delta^{(s)}(x', \theta', \phi') \quad (3.14)$$

is the smoothed density contrast in redshift space, which is convolved by an normalized kernel function W_R . The normalization of the kernel is given by

$$\int S_K^2(x') dx' \sin \theta' d\theta' d\phi' W_R(x, \theta, \phi; x', \theta', \phi') = 1. \quad (3.15)$$

The kernel function $W_R(x, \theta, \phi; x', \theta', \phi')$ is non-zero only when the comoving separation between (x, θ, ϕ) and (x', θ', ϕ') is comparable to, or less than R . Practically, R is much less than the Hubble scale, and the linear operator in the equation (B24) is commutable with the smoothing integration of equation (3.14), since the functions $D(z)$, $b(z)$, $f(z)$, $\alpha(z)$, and $S_K(x)$ are practically constants over individual cells, and the Laplacian is an Hermitian operator. Therefore, the equation (3.14) reduces to

$$\delta_R^{(s)}(x(z), \theta, \phi) = D(z) \left\{ b(z) + f(z) \left[\frac{\partial}{\partial x} + \alpha(z) \right] \frac{\partial}{\partial x} (\Delta + 3K)^{-1} \right\} \delta_R(x(z), \theta, \phi), \quad (3.16)$$

where

$$\delta_R(x, \theta, \phi) = \int S_K^2(x') dx' \sin \theta' d\theta' d\phi' W_R(x, \theta, \phi; x', \theta', \phi') \delta(x', \theta', \phi'), \quad (3.17)$$

is the smoothed density contrast in real space. A complex shape of the smoothing kernel complicates further analytic treatment, and therefore slows down the numerical evaluation of the correlation matrix based on the analytic formula. It is desirable to choose the smoothing kernel as simple as possible. In this respect, the simplest choice of the smoothing function W_R is the spherically symmetric function in comoving space, in which case, the kernel is expanded by complete set of orthonormal modes X_0 (c.f., eq.[B10]),

$$W_R(x_{\text{rel}}) = \int \frac{k^2 dk}{2\pi^2} W(kR) X_0(k, x_{\text{rel}}), \quad (3.18)$$

where x_{rel} is the relative separation in comoving units between (x, θ, ϕ) and (x', θ', ϕ') . The equation (3.18) is inverted as

$$W(kR) = 4\pi \int S_K^2(x) dx W_R(x) X_0(k, x). \quad (3.19)$$

Since R is much less than the curvature scale, $R \ll |K|^{-1/2}$, the above equation accurately approximates to

$$W(kR) = 4\pi \int x^2 dx W_R(x) j_0(kx) = \int d^3x W_R(x) e^{-i\mathbf{k} \cdot \mathbf{x}} \quad (3.20)$$

Thus, the function $W(kR)$ is the Fourier transform of the kernel, or the spherical window function of the kernel. The popular choices are the top-hat window function $W(kR) = 3j_1(kR)/(kR) = 3(\sin kR - kR \cos kR)/(kR)^3$, and the Gaussian window function $W(kR) = \exp(-k^2 R^2/2)$. Useful window functions are given in Appendix C, including the m -weight Epanechnikov kernel, which might also be useful.

There is a useful addition theorem for X_l (e.g., Ratra & Peebles 1995; Matsubara 2000),

$$X_0(k, x_{\text{rel}}) = \sum_{l=0}^{\infty} (2l+1) X_l(k, x) X_l(k, x') P_l(\cos \theta_{\text{rel}}), \quad (3.21)$$

where X_l is given by equation (B6), $P_l(x)$ are the Legendre polynomials, θ_{rel} is the relative angle between the directions (θ, ϕ) and (θ', ϕ') . The sum rule (3.21) holds even for a non-flat case $K \neq 0$ as well as a flat case $K = 0$. The Legendre polynomials are also expanded by the spherical harmonics Y_l^m ,

$$P_l(\cos \theta_{\text{rel}}) = \frac{4\pi}{2l+1} \sum_{m=-l}^l Y_l^m(\theta, \phi) Y_l^{m*}(\theta', \phi'). \quad (3.22)$$

Combining equations (3.18), (3.21), and (3.22), the spherical kernel function W_R is explicitly represented by the arguments $(x, \theta, \phi; x', \theta', \phi')$ to be substituted into equation (3.17). The density contrast $\delta(x, \theta, \phi)$ in real space is also expanded by normal modes as in equation (B21). In this way, the integration by (x', θ', ϕ') in equation (3.17) is explicitly performed by orthogonal relations of equations (B3), (B9), resulting in

$$\delta_R(x, \theta, \phi) = \sum_{l,m} \int \frac{k^2 dk}{2\pi^2} W(kR) \tilde{\delta}_{lm}(k) X_l(k, x) Y_l^m(\theta, \phi). \quad (3.23)$$

This equation is a familiar one in the Fourier-Bessel expansion of smoothed fields in the flat universe, and is a natural extension to the non-flat universe, in general. The expansion (3.23) has just the same form as in the unsmoothed field of equation (B21), with the replacement of $\tilde{\delta}_{lm}(k) \rightarrow W(kR) \tilde{\delta}_{lm}(k)$. Consequently, the similar derivation of the unsmoothed correlation function in redshift space applies and the result of the smoothed correlation function is just given by the replacement $P(k) \rightarrow W^2(kR)P(k)$ in the final expression of the unsmoothed expression in Appendix B [eqs. (B27)–(B38)]. As a result, the correlation matrix (3.13) in redshift space with spherical cells of a fixed smoothing radius R in comoving space is given by

$$\xi_{ij}^{(s)} = b_i b_j D_i D_j \sum_{n=0}^2 \sum_{l=0}^{2n} c_l^{(n)}(x_i, x_j, \theta_{ij}) \xi_l^{(n)}(x_{ij}), \quad (3.24)$$

where

$$\xi_l^{(n)}(x) \equiv \frac{(-1)^n}{S_K^{2n-l}(x)} \int \frac{k^2 dk}{2\pi^2} \frac{\sqrt{N_l(k)}}{k(k^2 - 4K)^n} X_l(k, x) W^2(kR) P(k), \quad (3.25)$$

the factor $N_l(k)$ is given by equation (B7) and the functions $c_l^{(n)}(x_i, x_j, \theta_{ij})$ are given by equations (B30)–(B38). These equations, i.e., equations (3.24), (3.25), (B30)–(B38) are sufficient to construct a correlation matrix. The functions $c_l^{(n)}$ are given by elementary functions and the numerical evaluations are very fast. Although the functions $\xi_l^{(n)}$ involve integrations, this one-dimensional function is a common function to obtain the correlation matrix for a fixed cosmological model. Once the functions $\xi_l^{(n)}$ are evaluated and tabulated, one can use appropriate interpolations without integrations cell by cell. Therefore, one can make the evaluation of $\xi_l^{(n)}(x_{ij})$ a very fast procedure. These form our main technique of the fast construction of the correlation matrix.

The simplicity of constructing the correlation matrix is largely dependent of restricting ourselves in linear theory. On nonlinear scales, the shape of the power spectrum is evolving, and the redshift distortions are not properly described by predictions of linear theory. To ensure the nonlinearity does not have significant effects, one should carefully choose the KL modes which are described by linear theory. This is achieved by calculating Fourier spectra of KL modes in individual survey (see, e.g., Pope et al. 2004).

In practice, the comoving separations x_{ij} are usually not comparable to the curvature scale of the universe. Observationally, $|\Omega_{K0}|$ is less than 0.04 (Bennett et al. 2003; Spergel et al. 2003), which means the curvature scale is approximately five times larger than the Hubble scale, $|K|^{-1/2} \gtrsim 5c/H_0$. The clustering scale we observe is usually much smaller than the Hubble scale. In this case, we can safely put $K \rightarrow 0$ in the equation (3.25), since $x_{ij} \ll |K|^{-1/2}$. That is,

$$\xi_l^{(n)}(x) = \frac{(-1)^{n+l}}{x^{2n-l}} \int \frac{k^2 dk}{2\pi^2} \frac{j_l(kx)}{k^{2n-l}} W^2(kR) P(k), \quad (3.26)$$

when $x \ll |K|^{-1/2}$. Even in this approximation, the effect of curvature on the separation between the observer and the sample, $x_i = x(z_i)$, are still included through the coefficients $c_l^{(n)}$. The terms with a factor $|K|S_K^2(x_{ij})$ in $c_l^{(n)}$'s can also be neglected when the above approximation $x_{ij} \ll |K|^{-1/2}$ is applied.

In the shallow redshift surveys, where $z_i \ll 1$ for all cells, one can totally neglect the curvature effect not only in x_{ij} , but also in x_i . Consequently, the relative distance x_{ij} is simply given by $x_{ij}^2 = x_i^2 + x_j^2 - 2x_i x_j \cos \theta_{ij}$. The distances are just given by the redshifts, $x_i = cz_i/H_0$, which does not depend on any cosmological parameter when distances are measured in units of $h^{-1}\text{Mpc}$. The quantity γ_{ij} defined in equation (B40) is reduced to $\gamma_{ij} = (x_i - x_j \cos \theta_{ij})/x_{ij}$ and the quantity $\tilde{\theta}_{ij}$ in equation (B41) is simply given by $\tilde{\theta}_{ij} = \theta_{ij}$. In the expression of the coefficients $c_l^{(n)}$ of equations (B30)–(B38), one can replace $\beta_i = \beta_j = \beta_0 \equiv \beta(0)$, and the terms proportional to $|K|S_K^2(x_{ij})$ are negligible. The function $\alpha(z)$ in the equation (B25) or (B26) is predominantly determined by the variation of the selection function $\Phi(z)$ or $n(z)$ in the sample, so that the factor A_{ij} in the equation (B39) is given by

$$A_{ij} = \frac{x_{ij}}{x_i} \left\{ 2 + \frac{d \ln \Phi(z)}{d \ln z} \Big|_{z_i} \right\} = \frac{x_{ij}}{x_i} \frac{d \ln n(z)}{d \ln z} \Big|_{z_i} \quad (3.27)$$

The resulting formula of the correlation function is equivalent to the expression derived by Szalay, Matsubara & Landy (1998). The simplicity of the shallow surveys is that the correlation matrix depends polynomially on $\beta_0 = f(0)/b(0)$, and that there are no other dependences on the cosmological parameters, when the power spectrum is given.

In the limit $x_{ij} \ll x_i, x_j$, the distant-observer approximation is fulfilled, which drastically reduces the complexity of the formula (Matsubara 2000). In this limit, one can reasonably assume that the quantity $H(z)D(z)f(z)n(z)$ in the equation (B26) is approximately the same at z_i and z_j so that $A_{ij} = 0$ in the equation (B39). In the same limit, the approximation $\gamma_{ij} = \pi - \gamma_{ji}$, and $\cos \tilde{\theta}_{ij} = 1$ are followed. As a result, the coefficients $c_l^{(n)}$ of equations (B30)–(B38) survive only for

$$c_0^{(0)} = 1 + \frac{1}{3}(\beta_i + \beta_j) + \frac{1}{5}\beta_i\beta_j, \quad (3.28)$$

$$c_2^{(1)} = \left[\frac{2}{3}(\beta_i + \beta_j) + \frac{4}{7}\beta_i\beta_j \right] P_2(\cos \gamma), \quad (3.29)$$

$$c_4^{(2)} = \frac{8}{35}\beta_i\beta_j P_4(\cos \gamma), \quad (3.30)$$

where P_l are the Legendre polynomials, and $\gamma \equiv \gamma_{ij}$ is the angle between the line of sight and the separation x_{ij} . Although the distant-observer approximation is simpler, it is not appropriate in wide-angle redshift surveys. The general formula has more terms than the distant-observer approximation. However, this does not bring any significant problem to numerical evaluations of the correlation matrices.

As an illustration, the resulting smoothed correlation functions calculated by our methods are plotted in Figure C1. We assume the cosmological parameters are those of the concordance model, $\Omega_{M0} = 0.3$, $\Omega_{K0} = 0$, $w = -1$, $h = 0.7$, $f_{\text{baryon}} = 0.15$, $b = 1$, $\sigma_8 = 1$, where the Hubble constant in units of 100km/s/Mpc , h , the baryon fraction f_{baryon} , and the normalization of the mass fluctuations σ_8 are needed only for modeling the CDM + baryon power spectrum $P(k)$ (we used the fitting formula by Eisenstein & Hu 1998). The smoothing radius is $15 h^{-1}\text{Mpc}$. In the Figure, the contour lines of the correlation function around centers at redshifts $z = 0.04, 0.1, 0.2, 0.3, 0.4, 0.5, 1, 1.5, 2$ are plotted. The plots are in “ z -space” where the observer is sitting at the origin (0,0). More precisely, the contour lines indicates the values of the correlation matrix $\xi_{ij}^{(s)}$, where z_i takes the above discretized values. The remaining variables z_j and θ_{ij} correspond to the coordinates ($z_j \sin \theta_{ij}, z_j \cos \theta_{ij}$) in the Figure.

At low redshifts, the deviations from the distant-observer approximation are apparent. Thoughtless application of the distant-observer approximation results in a fatal error. Although one can still choose parameterization in low-redshift correlations to obtain better results, our method is free from this ambiguity.

There are prominent bumps in the contours which makes the contours look peculiar. These bumps are attributed to the baryon oscillation in the power spectrum. In fact, the real-space correlation function $\xi(x)$ has the corresponding bump on the scale of around $100 h^{-1}\text{Mpc}$, as shown in Figure C2. The thick curves correspond to the correlation function of the model which is equivalent to that used in Figure C1. There is a sharp peak on the scale of $100 h^{-1}\text{Mpc}$. This peak does not exist when $f_{\text{baryon}} = 0$, as also shown in the Figure.

When the smoothing is applied, the sharpness of the peak is reduced, and this “baryon peak” will be more like “baryon shoulder” in the correlation function. This baryon shoulder introduces a scale on the correlation function, which can be used as a “standard ruler” to measure the geometry of the universe (Matsubara & Szalay 2003; Blake & Glazebrook 2003; Seo & Eisenstein 2003). The location of the baryon peak in $\xi(x)$ is sensitive to the parameter $\Omega_{M0}h$ which determine the horizon size at the time of equality. The amplitude of the peak is sensitive to the parameter f_{baryon} which determine the strength of the baryon oscillation. Because the geometry of the universe determines the apparent scale of the baryon shoulder, the observation of ξ_{ij} constrains the geometry, almost irrespectively of the value of f_{baryon} (Matsubara & Szalay 2002).

3.3. Spherical Approximations of the Kernel

In the construction of the correlation matrix in the previous subsection, we have assumed the sphericity of the kernel in comoving space. In reality, the comoving distance–redshift relation and the curvature of the universe is needed in order to define a cell in redshift space, that has spherical comoving shape. This means that we have to assume the parameters Ω_{M0} , Ω_{Q0} , and $w(z)$ to exactly set the spherical shape. If we assume a wrong geometry, the assumed comoving space is

elongated or squashed to the line-of-sight direction. As a result, we end up with spheroidal cells in comoving space. One of the important application of calculating the correlation matrix in this paper is to determine cosmological parameters by Bayesian analysis, so that the uncertainty in setting spherical cells above is not desirable. However, the calculation of the correlation matrix for spheroidal cells is more complicated than spherical cells. The higher-order multipoles of the spheroidal cells cause an additional convolution in the expression (3.23). The simplicity of the correlation matrix is not preserved in that case, and thus the numerical computation of the correlation matrix will be significantly slowed down.

However, such elongation or squashing does not significantly change the value of the correlation matrix. The elements of the correlation matrix for pairs of distant cells are virtually unchanged, since the correlation function is a smooth function and the elements of the correlation matrix for distant cells are virtually the same as a bare values of the correlation function without smoothing. The elements of the correlation matrix for nearby cells are affected by a shape of the cells, although the effect is not expected to be large as long as the elongation or squashing is not large.

Keeping the simplicity of the expression of the correlation matrix, we introduce an approximate method to calculate the correlation matrix using spherical cells even when the assumed geometry is not exactly true. In this method, first we adopt a best guess of the geometry with assumed set of parameters, Ω_{M0} , Ω_{Q0} , and $w(z)$. The KL-mode projection in the Bayesian analysis explained in the previous section also needs a fiducial cosmological model, so that it might be natural to take the same parameters as for that fiducial model, although it is not necessary. Next we set the cells in observed redshift space to be spherical in the comoving space of the assumed geometry, and construct a data vector by galaxy counts in these cells. The assumed model to construct the data vector will be called the “map model” below. The cell radius R is defined in this map model.

In the Bayesian analysis, the data vector is fixed throughout the parameter estimation where cosmological parameters are varied. The parameters in the map model are generally not the same as the various cosmological parameters to be tested in the analysis. Therefore, the shape of the cells in the constructed data vector is not exactly spherical in each cosmological model to be tested, and is generically distorted to spheroids. In our approximation, the spheroidal shape in each cosmological model is approximated to the spherical shape with the same volume as the actual spheroids. The volume of the spheroids are given by

$$V_{\text{spheroids}}(z) = \left[\frac{D_A(z)}{D_A^{(\text{map})}(z)} \right]^2 \frac{H^{(\text{map})}(z)}{H(z)} \frac{4\pi R^3}{3}, \quad (3.31)$$

where $H^{(\text{map})}(z)$ and $D_A^{(\text{map})}(z)$ are the Hubble parameter and the comoving angular diameter distance of the map model, and $H(z)$ and $D_A(z)$ are the counterparts of the tested model in the parameter estimation. The spheroidal cell is approximated to the spherical cell of the effective radius,

$$R_{\text{eff}}(z) = \left[\frac{D_A(z)}{D_A^{(\text{map})}(z)} \right]^{2/3} \left[\frac{H^{(\text{map})}(z)}{H(z)} \right]^{1/3} R. \quad (3.32)$$

Since this kind of the shape correction is necessary only for nearby cells, and the effective radius is almost the same for nearby cells, we do not need to consider the smoothing integration of the cross correlation with different smoothing radius, in practice. Interpolation of the correlation matrices with several effective smoothing radii is sufficient when the map model and the tested model is not too different. In defining the map model, it is natural to use the same cosmological parameters as in constructing the projection matrix P . Therefore, when the analysis is iterated with respect to optimizing the projection matrix, it is preferable that the cosmological parameters of the map model are also iterated, even though it is not strictly necessary.

3.4. Insignificance of the Finger-of-God Effects on Linear Scales

While the linear velocity field induces only the coherent motion of galaxies, random velocities are also present in the nonlinear regime, and the clustering shape in redshift space is elongated in the direction of line of sight. This is the famous finger-of-God effect which is not described by the linear formula. How does the finger-of-God affect on the correlation matrix? Since the finger-of-God effect decreases with distances between centers of the cells, the maximal effect is on the identical cells, that is, on the variance $\sigma^2(R, z) = \xi_{ii}^{(s)}$. Consequently, we can estimate the maximal influence of the finger-of-God effect on the correlation matrix by the same effect on the variance.

The finger-of-God effect can be analytically modeled by incoherent peculiar velocities on small scales (Peacock 1992; Peacock & Dodds 1994). We can safely use the distant-observer approximation in this case. When the incoherent motion along the line of sight is empirically fitted by an exponential distribution function, $f(v) = \exp(-\sqrt{2}|v|/\sigma_p)/(\sqrt{2}\sigma_p)$ (Davis & Peebles 1983), the power spectrum with the finger-of-God effect is given by (Park et al. 1994)

$$P_{\text{FOG}}(k, \mu) = \frac{P(k)}{(1 + k^2 \mu^2 \sigma_F^2/2)^2}, \quad (3.33)$$

where μ is the direction cosine of the wavevector \mathbf{k} with respect to the line of sight, and $\sigma_F = \sigma_p/H(z)$ is the rms of the displacement in redshift space by incoherent velocities. The element of the correlation matrix, including linear redshift-distortion, is therefore modeled by

$$\xi_{ij} = \int \frac{d^3k}{(2\pi)^3} e^{i\mathbf{k} \cdot \mathbf{x}_{ij}} W^2(kR) \left(\frac{1 + \beta \mu^2}{1 + k^2 \mu^2 \sigma_F^2/2} \right)^2 P(k), \quad (3.34)$$

where $\mathbf{x}_{ij} = \mathbf{x}_i - \mathbf{x}_j$, $\mu = k_{\parallel}/k$ and k_{\parallel} is the line-of-sight component of the wavevector \mathbf{k} . Adopting the polar coordinates $\mathbf{k} = k(\sin \theta \cos \phi, \sin \theta \sin \phi, \cos \theta)$ in k -space, and setting $\mathbf{x}_{ij} = (x_{\perp}, 0, x_{\parallel})$, the ϕ -integration can be analytically performed to give

$$\xi_{ij} = \int \frac{k^2 dk}{2\pi^2} W^2(kR) P(k) \int_{-1}^1 \frac{d\mu}{2} \cos(kx_{\parallel}\mu) J_0(kx_{\perp}\sqrt{1-\mu^2}) \left(\frac{1 + \beta\mu^2}{1 + k^2\mu^2\sigma_F^2/2} \right)^2. \quad (3.35)$$

The dimensionality of the above integration will not be analytically reduced further for arbitrary separation \mathbf{x}_{ij} . The integrand is a strongly oscillating function, so that the two-dimensional integration will be a slow process.

However, the correction of the finger-of-God effect is not necessarily needed as we will see below. The finger-of-God effect erases the clustering on scales smaller than σ_F . Observationally, the velocity dispersion is approximately given by the figure $\sigma_p = 340 \text{ km/s}$ (Davis & Peebles 1983) for $z = 0$. This dispersion corresponds to $\sigma_F = 3.4 h^{-1} \text{ Mpc}$, which is smaller than the nonlinearity scale, $R \sim 10 h^{-1} \text{ Mpc}$ for $z = 0$. Therefore, the finger-of-God effect is expected to be smaller than the nonlinear effect on the clustering on average. Higher redshift regions have lower σ_p so that the finger-of-God effect is less significant.

To find more quantitative estimates of what is the finger-of-God effect on the correlation matrix, we compare the variance with and without the finger-of-God effect. The non-diagonal elements of the correlation matrix are less affected. The variance $\sigma^2(R)$ is given by substituting $x_{\perp} = x_{\parallel} = 0$ in the equation (3.35), and the μ -integration can be analytically performed to give (Cole, Fisher, & Weinberg 1995)

$$\begin{aligned} \sigma^2(R) = \frac{1}{2} \int \frac{k^2 dk}{2\pi^2} & \left\{ \frac{1}{1 + k^2\sigma_F^2/2} + \frac{\text{Arctan}(k\sigma_F/\sqrt{2})}{k\sigma_F/\sqrt{2}} \right. \\ & - \frac{2}{k^2\sigma_F^2/2} \left[\frac{1}{1 + k^2\sigma_F^2/2} - \frac{\text{Arctan}(k\sigma_F/\sqrt{2})}{k\sigma_F/\sqrt{2}} \right] \beta \\ & \left. + \frac{3}{k^4\sigma_F^4/4} \left[\frac{1 + k^2\sigma_F^2/3}{1 + k^2\sigma_F^2/2} - \frac{\text{Arctan}(k\sigma_F/\sqrt{2})}{k\sigma_F/\sqrt{2}} \right] \beta^2 \right\} W^2(kR) P(k). \end{aligned} \quad (3.36)$$

Taking the limit $\sigma_F \rightarrow 0$, a familiar amplification factor $1 + 3\beta/2 + \beta^2/5$ appears (Kaiser 1987). Focusing only on the finger-of-God effect, we set $\beta = 0$ for the moment. As an illustration, the variance in real space and in redshift space (with only the finger-of-God effect) are shown in Table 1. We take a power-law spectrum $P(k) \propto k^{-1.2}$ which corresponds to observations in nonlinear regime. The normalization $\sigma(R = 8 h^{-1} \text{ Mpc}) = 1$, and the velocity dispersion $\sigma_p = 340 \text{ km/s}$ are adopted, which match the observations (Davis & Peebles 1983). The power spectrum on large scales deviates from the power-law spectrum. In Table 2 the results for the cold dark matter (CDM) spectrum with a fitting formula of Eisenstein & Hu (1998) are shown. The damping by the finger-of-God does not dominate the linear infall effect on larger scales. The linear infall effect enhances the variance by a factor $1 + 3\beta/2 + \beta^2/5$. When $\Omega_{M0} = 0.3$ and $b = 1$, the enhancement factor is 37%, and when $b = 2$, the factor is 17%. These figures are always larger than the finger-of-God effect when $R \gtrsim 10 h^{-1} \text{ Mpc}$.

The dynamical nonlinear effect on the variance is actually larger than the finger-of-God effect. In fact, the nonlinear correction to the variance with smoothing is of order σ_L^2 , where σ_L^2 is the variance of the linear theory. For example, the nonlinear loop correction to the variance without smoothing is given by $\langle \delta^2 \rangle = \sigma_L^2 + 1.82\sigma_L^4$ (Scoccimarro & Frieman 1996). From Table 1, we see that the order of nonlinear corrections are always larger than the order of finger-of-God corrections by about a factor of five. Even when the radius of the cell R is still on nonlinear scales, the KL-mode projection can only leave the linear regime. In which case, the nonlinear correction is not needed in the evaluation of the correlation matrix, neither is the finger-of-God effect.

3.5. Correlation Matrices in Projected Samples on the Sky

When only the position on the sky is catalogued and the redshifts of galaxies are not observed, the data vector is a set of galaxy counts on the 2-dimensional sky, projected along the line of sight with some redshift distribution function $n(z)$. When the redshifts are totally unobserved, the selection function spreads over a wide redshift range. With photometric redshift data, the selection function can be chosen so that the selection is approximately uniform in some narrower redshift range and rapidly drops outside that range.

TABLE 1
THE FINGER-OF-GOD EFFECT ON THE VARIANCE FOR THE POWER-LAW MODEL WITH $n = -1.2$.

$R(h^{-1} \text{ Mpc})$	5	10	15	20	30	50
$\sigma_{\text{real}}^2(R)$	2.3	0.67	0.32	0.19	9.3×10^{-2}	3.69×10^{-2}
$\sigma_{\text{FOG}}^2(R)$	1.7	0.59	0.30	0.18	9.1×10^{-2}	3.66×10^{-2}
difference	28%	12%	6.4%	4.0%	2.0%	0.8%

One of the advantage of the projected sample is the absence of redshift-distortions. The correlation matrix is given by just integrating the angular correlation function $w(\theta)$. Handling the correlation matrix is thus simpler than the 3D sample. When the 2D smoothing kernel is circularly symmetric, the elements of the correlation matrix are represented by just a function of the distance between centers of cells. Therefore, the advantage of the circular cells is obvious. We consider an efficient method to obtain 2D correlation matrices for the circularly symmetric cells below.

In projected samples on the sky, the angular correlation function $w(\theta)$ is given by

$$w(\theta) = \int_0^\infty dz_1 dz_2 n(z_1) n(z_2) D(z_1) D(z_2) b(z_1) b(z_2) \xi[x(z_1, z_2, \theta)], \quad (3.37)$$

where $x(z_1, z_2, \theta)$ is the comoving distance between two points with redshifts z_1 and z_2 , and with an opening angle θ . This function is given by a geometric relation,

$$S_K^2[x(z_1, z_2, \theta)] = S_K^2[x(z_1)] + S_K^2[x(z_2)] - 2C_K[x(z_1)]C_K[x(z_2)]S_K[x(z_1)]S_K[x(z_2)]\cos\theta - K S_K^2[x(z_1)]S_K^2[x(z_2)](1 + \cos^2\theta), \quad (3.38)$$

where $x(z)$ is the comoving distance-redshift relation of equation (3.4). The selection function $n(z)$ is the normalized redshift distribution dN/dz of galaxies with

$$\int_0^\infty dz n(z) = 1. \quad (3.39)$$

The volume factor is included in $n(z)$ so that the relation to the selection function per comoving volume $\Phi(z)$ is given by $H(z)n(z) \propto S_K^2[x(z)]\Phi(z)$. The correlation function in real space $\xi(x)$ is given by

$$\xi(x) = \int \frac{k^2 dk}{2\pi^2} \frac{\sin kx}{k S_K(x)} P(k), \quad (3.40)$$

which is derived from equations (B21), (3.21) and (3.22) [the equivalent formula of $\xi(x)$ for an open universe is given in Wilson (1983)].

The direct 2-dimensional integration of equation (3.37) is numerically straightforward and relatively fast, once the 3-dimensional correlation function $\xi(x)$ is tabulated and interpolated. In this integration, we should use a dense sampling for small separation, $x(z_1, z_2, \theta)$, for a fast calculation. For example, the integration variable z_2 for a fixed z_1 can be transformed to $y_\pm = |z_2 - z_1| + 2z_1 \sin(\theta/2)$. According to the sign of $z_2 - z_1$ we use y_+ and y_- respectively. Logarithmically uniform sampling in y_\pm -integration can achieve the dense sampling for small separations. In this paper, we follow this strategy in numerically evaluating the equation (3.37). The result of the numerical integration for a concordance model, $\Omega_{M0} = 0.3$, $\Omega_{K0} = 0$, $w = -1$, $h = 0.7$, $f_{\text{baryon}} = 0.15$, $b = 1$, $\sigma_8 = 1$ is shown on Figure C3 by a solid line. The selection function is simply taken as a step-wise function, $n(z) = \text{const.}$ for $0.5 < z < 1$ and $n(z) = 0$ otherwise. In the angular correlation function, the baryon peak in $\xi(x)$ is almost erased, although there is a hint of a bump around 100–200 arcmin.

The signal part of the correlation matrix is given by the smoothing integration of $w(\theta)$:

$$w_{ij} = \int \sin\theta d\theta d\phi \int \sin\theta' d\theta' d\phi' W_i(\theta, \phi) W_j(\theta', \phi') w(\theta_{\text{rel}}), \quad (3.41)$$

where $W_i(\theta, \phi)$ is the smoothing kernel of a cell i with a unit normalization, and θ_{rel} is the angle between directions (θ, ϕ) and (θ', ϕ') . When the smoothing kernel does not have simple shape, or varies from cell to cell, the straightforward evaluation of the correlation matrix is given by directly integrating equations (3.37) and (3.41). Firstly, the correlation function $\xi(x)$ is calculated and tabulated. Secondly, using the interpolation of the tabulated $\xi(x)$, the two-dimensional integration of equation (3.37) yields the angular correlation function $w(\theta)$ which is again tabulated. Finally, the four-dimensional integration of equation (3.41) provides the correlation matrix.

However, the above procedure is not a fast process because the smoothing integration involves a four-dimensional integration cell by cell. In the philosophy that the numerical computation of the correlation matrix should be maximally reduced, it is better to choose the shape of the cells as in the three dimensional analysis of the redshift surveys. The simplest choice is the circularly symmetric kernel $W_{\theta_s}(\theta)$ where θ is the relative angle from a center of a kernel, θ_s is the angular smoothing scale. The normalization of this kernel is given by

$$2\pi \int_0^\infty \sin\theta d\theta W_{\theta_s}(\theta) = 1 \quad (3.42)$$

TABLE 2

THE FINGER-OF-GOD EFFECT ON THE VARIANCE FOR THE CDM MODEL WITH $\Gamma = 0.2$.

$R(h^{-1}\text{Mpc})$	5	10	15	20	30	50
$\sigma_{\text{real}}^2(R)$	1.9	0.71	0.36	0.22	8.4×10^{-2}	3.50×10^{-2}
$\sigma_{\text{FOG}}^2(R)$	1.5	0.64	0.34	0.21	8.3×10^{-2}	3.46×10^{-2}
difference	22%	10%	5.3%	4.8%	1.5%	1.2%

In this case, the elements of the correlation matrix w_{ij} depend only on the angular separation of the cells, θ_{ij} , i.e., $w_{ij} = u(\theta_{ij})$. Once the function $u(\theta)$ is calculated and tabulated, the correlation matrix is obtained by simple interpolations, which are very fast procedures.

The straightforward representation of the function $C(\theta)$ is provided by the standard multipole expansion:

$$u(\theta) = \sum_{l=0}^{\infty} \frac{2l+1}{4\pi} P_l(\cos \theta) |W_l|^2 C_l, \quad (3.43)$$

where C_l is the angular power spectrum and W_l is the multipole of the circular window function

$$W_l = 2\pi \int_0^\pi \sin \theta d\theta W_{\theta_s}(\theta) P_l(\cos \theta), \quad (3.44)$$

The angular power spectrum is related to the spatial power spectrum $P(k)$ by

$$C_l = 4\pi \int_0^\infty \frac{k^2 dk}{2\pi^2} |\Psi_l(k)|^2 P(k), \quad (3.45)$$

where $\Psi_l(k)$ is defined by

$$\Psi_l(k) = \int_0^\infty dz n(z) D(z) b(z) X_l[k, x(z)], \quad (3.46)$$

and $x(z)$ is given by equation (3.4). Numerical evaluation of this expression is not so fast, because integrations over k and z and sum over l are involved for oscillating functions, X_l and P_l . In addition, numerical evaluations of $X_l(k, x)$ might be tricky for a non-flat universe. Thus, it is better to seek a more efficient method to numerically evaluate the function $u(\theta)$.

If the angle θ is sufficiently small and the flat-sky approximation can be applied, the angular correlation function is given by Limber's equation (Peebles 1980)

$$w(\theta) = \int_0^\infty dz H(z) n^2(z) D^2(z) b^2(z) \int_0^\infty \frac{k dk}{2\pi} J_0[k\theta D_A(z)] P(k), \quad (3.47)$$

where $D_A(z) = S_K[x(z)]$ is the comoving angular diameter distance, and $J_\nu(x)$ is the Bessel function. This approximation is compared to the exact integration of equation (3.37) in Figure C3. As one can see, Limber's equation is reasonably accurate for $\theta \lesssim 100$ arcmin. ~ 1.7 degrees within 0.5% for the concordance model.

The two-dimensional Fourier transform (in the flat-sky approximation) of the angular correlation function is given by

$$\tilde{w}(l) = \int d^2\theta e^{-i\mathbf{l}\cdot\boldsymbol{\theta}} w(\theta) = 2\pi \int_0^\infty \theta d\theta J_0(l\theta) w(\theta) = \int_0^\infty dz \frac{H(z) n^2(z) D^2(z) b^2(z)}{d_{cA}^2(z)} P\left(\frac{l}{d_{cA}(z)}\right), \quad (3.48)$$

where the completeness relation of the Bessel function (e.g., Arfken & Weber 2001),

$$\int_0^\infty x dx J_\nu(ax) J_\nu(bx) = \frac{1}{a} \delta(a - b) \quad (\nu > -1/2) \quad (3.49)$$

is used. The two-dimensional Fourier window function is given by

$$W(l\theta_s) = \int d^2\theta e^{-i\mathbf{l}\cdot\boldsymbol{\theta}} W_{\theta_s}(\theta) = 2\pi \int_0^\infty \theta d\theta J_0(l\theta) W_{\theta_s}(\theta), \quad (3.50)$$

which should not be confused with the three-dimensional one in the previous subsection although we use the same notation. It is straightforward to show that $\tilde{w}(l) \simeq C_l$ and $W(l\theta_s) \simeq W_l$ in the limit of $l \gg 1$ because $P_l(\cos \theta) \simeq J_0(l\theta)$ in the same limit. The top-hat window function corresponds to $W(l\theta_s) = 2J_1(l\theta_s)/(l\theta_s)$. The smoothed angular correlation function $u(\theta)$ is the convolution of the angular correlation $w(\theta)$ with the smoothing kernel $W_{\theta_s}(\theta)$ for both ends, and consequently, using the convolution theorem, we have

$$\begin{aligned} u(\theta) &= \int_0^\infty \frac{ldl}{2\pi} J_0(l\theta) W^2(l\theta_s) \tilde{w}(l) \\ &= \int_0^\infty dz H(z) n^2(z) D^2(z) b^2(z) \int_0^\infty \frac{k dk}{2\pi} J_0[k\theta d_{cA}(z)] W^2[k\theta_s d_{cA}(z)] P(k). \end{aligned} \quad (3.51)$$

The numerical performance of this two-dimensional integration is reasonably fast because the integrand of the variable z is a smooth function. The integration by the variable k is fast as long as the effective spectral index of $P(k)$ is negative on the relevant scales which is indicated by the angle θ .

Limber's equation is not appropriate for wide-angle correlations. However, the smoothing angle θ_s is much smaller than the opening angle of the survey. In this case, we can apply flat coordinates within the smoothing cells, and the function $u(\theta)$ is straightforwardly represented by

$$\begin{aligned} u(\theta) &= \int \theta_1 d\theta_1 d\phi_1 \int \theta_2 d\theta_2 d\phi_2 W_{\theta_s}(\theta_1) W_{\theta_s}(\theta_2) \\ &\quad \times w \left[\sqrt{(\theta + \theta_2 \cos \phi_2 - \theta_1 \cos \phi_1)^2 + (\theta_2 \sin \phi_2 - \theta_1 \sin \phi_1)^2} \right]. \end{aligned} \quad (3.52)$$

This four-dimensional integration is not needed for a separation angle larger than the size of the cells, $\theta \gg \theta_s$, because the smoothing effect is small in that case, so that $u(\theta) = w(\theta)$ in the lowest (0th) order. Taylor expansion of the equation (3.52) with respect to θ_1/θ and θ_2/θ yields higher-order corrections to this simple approximation of the 0th order. The smoothing kernel of the form,

$$W_{\theta_s}(\theta) = \theta_s^{-2} W_s(\theta/\theta_s), \quad (3.53)$$

has a scaling with respect to the smoothing angle, where W_s is a single-variable function, independent on smoothing angle θ_s , and normalized by

$$2\pi \int_0^\infty t dt W_s(t) = 1. \quad (3.54)$$

Defining scaled moments of the kernel,

$$m_k \equiv 2\pi \int_0^\infty t dt t^k W_s(t), \quad (3.55)$$

the Taylor expansion of the equation (3.52) up to forth order is straightforwardly calculated to give

$$\begin{aligned} u(\theta) = w(\theta) &+ \frac{m_2}{2} \left[w''(\theta) + \frac{w'(\theta)}{\theta} \right] \theta_s^2 \\ &+ \frac{m_4 + 2m_2^2}{32} \left[w''''(\theta) + \frac{2w'''(\theta)}{\theta} - \frac{w''(\theta)}{\theta^2} + \frac{w'(\theta)}{\theta^3} \right] \theta_s^4 + \dots \end{aligned} \quad (3.56)$$

For a top-hat kernel, $W_{\theta_s}(\theta) = \Theta(\theta_s - \theta)/\pi\theta_s^2$, $W_s(t) = \Theta(1 - t)/\pi$ and $m_k = 1/(k/2 + 1)$ so that the numerical coefficients of second-order and forth-order terms are 1/4 and 5/192, respectively.

On Figure C4, the smoothed angular correlation functions $u(\theta)$ in the various approximations given above are compared when a top-hat kernel is adopted with a smoothing angle $\theta_s = 10$ arcmin. In the range of angles plotted here, the Limber's equation is accurate enough and the equation (3.51) gives practically exact result. The first-order approximation, in which the terms up to θ_s^2 in equation (3.56) are kept, well reproduce the exact result for $\theta \gtrsim 1.6\theta_s$. The second-order approximation does not significantly improve the first-order approximation. At $\theta = 2\theta_s$, fractional errors are 4%, 0.9%, and 0.3% for truncations of the Taylor series up to zeroth, first, and second orders, respectively. Therefore, one does not need to perform the four-dimensional numerical integration even for neighboring cells, as long as cells do not overlap. We only need to numerically evaluate the bare angular correlation function $w(\theta)$. Since the angular correlation function is practically a smooth function, the numerical evaluations of derivatives of $w(\theta)$ are stable enough once $w(\theta)$ is obtained.

Thus, in practice, only the self-correlation $w_{ii} = u(0)$ should be evaluated in some way other than the equation (3.56). This should be done only once, so that the direct four-dimensional numerical integration of equation (3.52) is still reasonable. Alternatively, since the Limber's equation is appropriate for the self-correlation, one can use the equation (3.51) with $\theta = 0$,

$$u(0) = \int_0^\infty dz H(z) n^2(z) D^2(z) b^2(z) \int_0^\infty \frac{k dk}{2\pi} W^2[k\theta_s d_{cA}(z)] P(k), \quad (3.57)$$

which is two-dimensional integration and is faster to compute than the direct four-dimensional integration.

Obtaining the one-dimensional function $u(\theta)$ by using appropriate methods explained above, the correlation matrix R_{ij} including the noise term is immediately constructed by (c.f., eq.[2.9])

$$R_{ij} = N_i N_j u(\theta_{ij}) + \sqrt{N_i N_j} K_{ij} + E_{ij}, \quad (3.58)$$

where θ_{ij} is the separation angle between cells i and j , E_{ij} is the correlation matrix for other sources of noise except the shot noise. The quantities N_i , K_{ij} are defined by

$$N_i = \int \sin \theta d\theta d\phi K_i(\theta, \phi) n(\theta, \phi), \quad (3.59)$$

$$K_{ij} = \frac{1}{S_i S_j} \int \sin \theta d\theta d\phi K_i(\theta, \phi) K_j(\theta, \phi), \quad (3.60)$$

where $n(\theta, \phi)$ is the mean number density of the 2D sample, which can depend on the direction because of possibly inhomogeneous sampling, $K_i(\theta, \phi)$ is the smoothing kernel of the cell i with an arbitrary normalization,

$$S_i = \int \sin \theta d\theta d\phi K_i(\theta, \phi). \quad (3.61)$$

The normalized kernel $W_i(\theta, \phi)$ in equation (3.41) is given by $W_i(\theta, \phi) = K_i(\theta, \phi)/S_i$ (no sum over i).

4. APPLICATION TO THE LIKELIHOOD ANALYSIS

4.1. Cosmological Parameters of Simple Dependence on the Correlation Matrices

In the likelihood analysis, one needs to repeatedly calculate the correlation matrices for models with various parameters. The methods to calculate the correlation matrices described above are already fast. However, when the dependence on some cosmological parameter is linear or polynomial, the repeated compression of the correlation matrix R into a reduced

matrix C of equation (2.5) is not necessarily needed in changing that parameter. Generally, if the dependence of a cosmological parameter θ on the correlation matrix has the form,

$$R = R^{(0)} + R^{(1)}\theta + R^{(2)}\theta^2 + \dots, \quad (4.1)$$

where $R^{(k)}$'s do not depend on θ , then the reduced correlation matrix of equation (2.5) is given by

$$C = C^{(0)} + C^{(1)}\theta + C^{(2)}\theta^2 + \dots, \quad (4.2)$$

where

$$C^{(k)} = PR^{(k)}P^T, \quad (4.3)$$

and P is the projection matrix of equation (2.4). Therefore, when the partial matrices $C^{(k)}$ are calculated fixing other parameters, one can omit the projection of the huge matrix in changing the particular parameter θ . Instead, the reduced correlation matrix C is obtained simply by a summation of equation (4.3).

The obvious example of the cosmological parameter which has the polynomial dependence on correlation matrices is the normalization parameter of the mass power spectrum, σ_8^2 , or A_s . The signal part of the correlation matrix, ξ_{ij} , or w_{ij} is always proportional to this parameter. The correlation matrix of a redshift survey is written as

$$R_{ij} = \sigma_8^2 N_i N_j \hat{\xi}_{ij} + \sqrt{N_i N_j} K_{ij} + E_{ij} \quad (4.4)$$

where $\hat{\xi}_{ij}$ is the signal part of the correlation matrix of equation (3.24) with the normalization $\sigma_8 = 1$.

The dependence on the parameter β at a fixed redshift is polynomial. To see this, the expression of the correlation matrix ξ_{ij} of equations (3.24) and (B30)–(B38) is re-arranged according to the dependences on β_i and β_j :

$$\xi_{ij} = b_i b_j D_i D_j \left(\xi_{ij}^{(0)} + \beta_i \xi_{ij}^{(1)} + \beta_j \xi_{ji}^{(1)} + \beta_i \beta_j \xi_{ij}^{(2)} \right) \quad (4.5)$$

$$= D_i D_j \left(b_i b_j \xi_{ij}^{(0)} + f_i b_j \xi_{ij}^{(1)} + f_j b_i \xi_{ji}^{(1)} + f_i f_j \xi_{ij}^{(2)} \right) \quad (4.6)$$

where $\xi_{ij}^{(k)}$ ($k = 0, 1, 2$) do not depend on β_i , β_j , or on b_i , b_j . The matrix $\xi_{ij}^{(1)}$ is not symmetric in general. It is straightforward to obtain $\xi_{ij}^{(k)}$. For convenience, below we give the explicit representation in the case of $x_{ij} \ll |K|^{-1/2}$, which is fulfilled in practice, since the curvature scale is observationally more than five times larger than the Hubble scale as discussed just above equation (3.26). In this case we can put $|K|S_K^2(x_{ij}) = 0$, $C_K(x_{ij}) = 1$ and $\tilde{\theta}_{ij} = \theta_{ij}$ in the equations (B30)–(B38). Therefore,

$$\xi_{ij}^{(0)} = \xi_0^{(0)}(x_{ij}), \quad (4.7)$$

$$\xi_{ij}^{(1)} = \frac{1}{3} \xi_0^{(0)}(x_{ij}) + A_{ij} \cos \gamma_{ij} \xi_1^{(1)}(x_{ij}) + \left(\cos^2 \gamma_{ij} - \frac{1}{3} \right) \xi_2^{(1)}(x_{ij}), \quad (4.8)$$

$$\begin{aligned} \xi_{ij}^{(2)} = & \frac{1}{15} (1 + 2 \cos^2 \theta_{ij}) \xi_0^{(0)}(x_{ij}) - \frac{1}{3} A_{ij} A_{ji} \cos \theta_{ij} \xi_0^{(1)}(x_{ij}) \\ & + \frac{1}{5} [A_{ij} (\cos \gamma_{ij} - 2 \cos \gamma_{ji} \cos \theta_{ij}) + A_{ji} (\cos \gamma_{ji} - 2 \cos \gamma_{ij} \cos \theta_{ij})] \xi_1^{(1)}(x_{ij}) \\ & - \frac{1}{7} \left[\frac{2}{3} + \frac{4}{3} \cos^2 \theta_{ij} - (\cos^2 \gamma_{ij} + \cos^2 \gamma_{ji}) + 4 \cos \gamma_{ij} \cos \gamma_{ji} \cos \theta_{ij} \right] \xi_2^{(1)}(x_{ij}) \\ & + A_{ij} A_{ji} \left(\cos \gamma_{ij} \cos \gamma_{ji} + \frac{1}{3} \cos \theta_{ij} \right) \xi_2^{(2)}(x_{ij}) \\ & + \frac{1}{5} [A_{ij} (5 \cos \gamma_{ij} \cos^2 \gamma_{ji} - \cos \gamma_{ij} + 2 \cos \gamma_{ji} \cos \theta_{ij}) \\ & \quad + A_{ji} (5 \cos \gamma_{ji} \cos^2 \gamma_{ij} - \cos \gamma_{ji} + 2 \cos \gamma_{ij} \cos \theta_{ij})] \xi_3^{(2)}(x_{ij}) \\ & + \frac{1}{7} \left[\frac{1}{5} + \frac{2}{5} \cos^2 \theta_{ij} - (\cos^2 \gamma_{ij} + \cos^2 \gamma_{ji}) + 4 \cos \gamma_{ij} \cos \gamma_{ji} \cos \theta_{ij} \right. \\ & \quad \left. + 7 \cos^2 \gamma_{ij} \cos^2 \gamma_{ji} \right] \xi_4^{(2)}(x_{ij}). \end{aligned} \quad (4.9)$$

The quantity $\xi_{ij}^{(0)}$ corresponds to the isotropic component of the correlations, since it depends only on x_{ij} . The quantities $\xi_{ij}^{(1)}$ and $\xi_{ij}^{(2)}$ are relevant to the distortions by the peculiar velocity field.

When a fixed redshift z_{pivot} is arbitrarily chosen, the correlation matrix is explicitly polynomial with respect to the parameter $\beta_{\text{piv}} \equiv \beta(z_{\text{pivot}})$:

$$\xi_{ij} = (b_{\text{piv}} D_{\text{piv}})^2 \hat{b}_i \hat{b}_j \hat{D}_i \hat{D}_j \left[\xi_{ij}^{(0)} + \beta_{\text{piv}} \left(\hat{\beta}_i \xi_{ij}^{(1)} + \hat{\beta}_j \xi_{ji}^{(1)} \right) + \beta_{\text{piv}}^2 \hat{\beta}_i \hat{\beta}_j \xi_{ij}^{(2)} \right], \quad (4.10)$$

where $b_{\text{piv}} \equiv b(z_{\text{pivot}})$ and $D_{\text{piv}} \equiv D(z_{\text{pivot}})$ are the bias and the growth factor at a pivot redshift. The relative evolutions with respect to z_{pivot} are represented by quantities $\hat{b}_i \equiv b(z_i)/b(z_{\text{pivot}})$, $\hat{D}_i \equiv D(z_i)/D(z_{\text{pivot}})$, and $\hat{\beta}_i \equiv \beta(z_i)/\beta(z_{\text{pivot}})$.

When the redshift range of the survey is not significantly large, the relative evolutions are small, and are not strongly varying functions of redshift.

It is not hard to imagine that the typical bias b_{pivot} and the overall normalization of the mass power spectrum at z_{pivot} , $\sigma_{8,\text{piv}} = D_{\text{piv}}\sigma_8$, contribute to the correlation matrix in similar way, and these parameters degenerate in estimating the likelihood function, although the distortion terms break this degeneracy to some extent. Since it is not advantageous to deal with almost degenerated parameters separately, it might be preferable to consider the normalization of the galaxy power spectrum at z_{pivot} , $\sigma_{8,\text{piv}} \equiv b_{\text{piv}}\sigma_8 = b_{\text{piv}}D_{\text{piv}}\sigma_8$, as an independent parameter instead of the unobservable σ_8 . We introduce the normalized correlations, $\hat{\xi}_{ij}^{(k)}$ ($k = 0, 1, 2$), which are calculated from the power spectrum with a normalization $\sigma_8 = 1$, so that $\xi_{ij}^{(k)} = \sigma_8^2 \hat{\xi}_{ij}^{(k)}$. The correlation matrix of equation (4.10) is then reduced to

$$R_{ij} = \sigma_{8,\text{piv}}^2 N_i N_j \hat{b}_i \hat{b}_j \hat{D}_i \hat{D}_j \left[\hat{\xi}_{ij}^{(0)} + \beta_{\text{piv}} \left(\hat{\beta}_i \hat{\xi}_{ij}^{(1)} + \hat{\beta}_j \hat{\xi}_{ji}^{(1)} \right) + \beta_{\text{piv}}^2 \hat{\beta}_i \hat{\beta}_j \hat{\xi}_{ij}^{(2)} \right] + \sqrt{N_i N_j} K_{ij} + E_{ij}, \quad (4.11)$$

(no sum over i, j). Thus the normalization of the galaxy power spectrum at the pivot redshift, $\sigma_{8,\text{piv}}$, and the redshift-distortion parameter at the pivot redshift, β_{piv} , are independent parameters both of which polynomially contribute to the correlation matrix. The parameters σ_8 and b_{piv} are dependent parameters through the relations

$$\sigma_8 = \frac{\sigma_{8,\text{piv}} \beta_{\text{piv}}}{f(z_{\text{pivot}}) D(z_{\text{pivot}})}, \quad (4.12)$$

$$b_{\text{piv}} = \frac{f(z_{\text{pivot}})}{\beta_{\text{piv}}}. \quad (4.13)$$

In similar ways, one can arbitrary choose two independent parameters out of σ_8 , b_{piv} , β_{piv} , and $\sigma_{8,\text{piv}}$, depending on individual analysis.

Each term in the equation (4.11) is separately projected to the reduced matrices as explained above. As detailed in Appendix A, the projection matrix P whitens the noise correlation matrix, and the reduced correlation matrix $C = PRP^T$ is given by

$$C_{nm} = \sigma_{8,\text{piv}}^2 \left(C_{nm}^{(0)} + \beta_{\text{piv}} C_{nm}^{(1)} + \beta_{\text{piv}}^2 C_{nm}^{(2)} \right) + \delta_{nm}, \quad (4.14)$$

where

$$C_{nm}^{(0)} = \sum_{i,j} P_{ni} P_{mj} N_i N_j \hat{b}_i \hat{b}_j \hat{D}_i \hat{D}_j \hat{\xi}_{ij}^{(0)}, \quad (4.15)$$

$$C_{nm}^{(1)} = \sum_{i,j} P_{ni} P_{mj} N_i N_j \hat{D}_i \hat{D}_j \left(\hat{f}_i \hat{b}_j \hat{\xi}_{ij}^{(1)} + \hat{f}_j \hat{b}_i \hat{\xi}_{ji}^{(1)} \right), \quad (4.16)$$

$$C_{nm}^{(2)} = \sum_{i,j} P_{ni} P_{mj} N_i N_j \hat{D}_i \hat{D}_j \hat{f}_i \hat{f}_j \hat{\xi}_{ij}^{(2)}. \quad (4.17)$$

Once the projections of the matrices in the equations (4.15)–(4.17) are obtained for a given set of parameters except $\sigma_{8,\text{piv}}$ and β_{piv} , the reduced correlation matrix C_{nm} is immediately derived by the equation (4.14) for any values of $\sigma_{8,\text{piv}}$ and β_{piv} without projecting the huge matrix again. Other cosmological parameters, including $\Omega_{\text{M}0}$, $\Omega_{\text{Q}0}$, and parameters which parametrize the evolution of the bias, $\hat{b}(z)$, and of the equation of state for the dark energy, $w(z)$, are non-polynomially dependent on the correlation matrix R_{ij} . The projection operation should be performed for each set of these non-polynomial parameters.

In shallow redshift surveys, however, the evolutionary effects of the cosmological quantities above are small. In this case, the natural choice of the pivot redshift is $z_{\text{pivot}} = 0$ so that $\sigma_{8,\text{piv}} = \sigma_8$ and $\beta_{\text{piv}} = \beta_0$. One can also approximately set $\hat{D} = 1$, $\hat{f} = 1$, $\hat{b} = 1$, and $H(z) = H_0$ in the formula of the correlation matrix (H_0 does not explicitly affect the correlation matrix in redshift space for a given power spectrum, only through the power spectrum). The only non-polynomial parameters are those which parametrize the power spectrum, since, with the good approximation, the distances are proportional to the redshifts and the geometry is flat. Therefore, in this case, the elements $\hat{\xi}_{ij}^{(k)}$ are fully determined where any dependence on cosmological parameters is only through the power spectrum. The representation of equations (4.15)–(4.17) are simplified as

$$C_{nm}^{(0)} = \sum_{i,j} P_{ni} P_{mj} N_i N_j \hat{\xi}_{ij}^{(0)}, \quad (4.18)$$

$$C_{nm}^{(1)} = \sum_{i,j} P_{ni} P_{mj} N_i N_j \left(\hat{\xi}_{ij}^{(1)} + \hat{\xi}_{ji}^{(1)} \right), \quad (4.19)$$

$$C_{nm}^{(2)} = \sum_{i,j} P_{ni} P_{mj} N_i N_j \hat{\xi}_{ij}^{(2)}, \quad (4.20)$$

which are only dependent on the shape of the power spectrum.

4.2. Band Power Estimation of the Power Spectrum

The correlation matrix is always linearly dependent on the power spectrum as long as the linear regime is considered. Therefore, decomposing the power spectrum into band powers can be used to straightforwardly estimate the power spectrum, without parameterizing the shape of the power spectrum (Tegmark, Hamilton, & Xu 2002). Below we briefly explain the band power estimation within the context of our method.

The power spectrum is decomposed into band powers as

$$P(k) = \sum_{p=1}^{n_p} A_p \hat{P}_p(k), \quad (4.21)$$

where $\hat{P}_p(k)$ is the band-power base function which has support near the wavenumber k_p , and A_p is the power of the band p . The choice of the band-power base function is not unique, as long as the power spectrum is parameterized by linear parameters A_p . The simplest choice is the piecewise constant functions,

$$\hat{P}_p(k) = \Theta(k_{p+1} - k)\Theta(k - k_p). \quad (4.22)$$

Another choice is the piecewise linear functions,

$$\hat{P}_p(k) = \frac{k - k_{p-1}}{k_p - k_{p-1}}\Theta(k_p - k)\Theta(k - k_{p-1}) + \frac{k_{p+1} - k}{k_{p+1} - k_p}\Theta(k_{p+1} - k)\Theta(k - k_p). \quad (4.23)$$

One can construct more complex bases by optimizing the band powers (e.g., see Hamilton 1997; Hamilton & Tegmark 2000). Each band contributes linearly to the reduced correlation matrix C_{nm} . We denote the contribution of each band p to the matrices $\xi_{ij}^{(a)}$ ($a = 0, 1, 2$) of equations (4.7)–(4.9) by $\xi_{ij}^{(a,p)}$ such that

$$\xi_{ij}^{(a)} = \sum_{p=1}^{n_p} A_p \xi_{ij}^{(a,p)}. \quad (4.24)$$

Then, analogously to the equations (4.14)–(4.17), the reduced correlation matrix is given by

$$C_{nm} = \sum_{a=0}^2 \sum_{p=1}^{n_p} A_p \beta_{\text{piv}}^a C_{nm}^{(a,p)} + \delta_{nm}, \quad (4.25)$$

where

$$C_{nm}^{(0,p)} = \sum_{i,j} P_{ni} P_{mj} N_i N_j \hat{b}_i \hat{b}_j \hat{D}_i \hat{D}_j \xi_{ij}^{(0,p)}, \quad (4.26)$$

$$C_{nm}^{(1,p)} = \sum_{i,j} P_{ni} P_{mj} N_i N_j \hat{D}_i \hat{D}_j \left(\hat{f}_i \hat{b}_j \xi_{ij}^{(1,p)} + \hat{f}_j \hat{b}_i \xi_{ji}^{(1,p)} \right), \quad (4.27)$$

$$C_{nm}^{(2,p)} = \sum_{i,j} P_{ni} P_{mj} N_i N_j \hat{D}_i \hat{D}_j \hat{f}_i \hat{f}_j \xi_{ij}^{(2,p)}. \quad (4.28)$$

The matrices $C_{nm}^{(a,p)}$ still depend on the cosmological parameters because of the evolutionary effects. However, in case of shallow surveys, they become independent on any parameters at all. Once the matrices $C_{nm}^{(a,p)}$ are obtained, the dependencies of the correlation matrix on parameters a_p and β_0 are explicitly polynomial.

4.3. Quadratic Estimator

When the number of parameters to be estimated is large, it is not realistic to calculate the likelihood function on every mesh point in the parameter space. When the behavior of the likelihood function is completely unknown, there are no safe methods to maximize the likelihood in parameter space. In the present application in cosmology, the correlation matrix smoothly varies with cosmological parameters in general. In this case, the likelihood function near a peak is approximated as a Gaussian. Therefore, as long as we approximately know the true cosmological parameters, one can reach the location of maximum likelihood by a few iterative steps using the Newton-Raphson method. This approach is taken by Bond, Jaffe, & Knox (1998) (hereafter, BJK) in estimating the power spectrum of the cosmic microwave background (CMB). The same method is also applied to the analysis of the 2-dimensional galaxy survey (Huterer, Knox & Nichol 2001; Efstathiou & Moody 2001). The purpose of this section is to give an aspect of applying BJK's method to the present analysis.

Following BJK, the likelihood function of equation (2.6), $\mathcal{L}(\{\theta_\alpha\}) \equiv P(D_{\text{reduced}}|\Theta)$ is approximated by a Gaussian:

$$\ln \mathcal{L}(\{\theta_\alpha + \delta\theta_\alpha\}) = \ln \mathcal{L}(\{\theta_\alpha\}) + \sum_{\alpha} \frac{\partial \ln \mathcal{L}}{\partial \theta_\alpha} \delta\theta_\alpha + \frac{1}{2} \sum_{\alpha, \beta} \frac{\partial^2 \ln \mathcal{L}}{\partial \theta_\alpha \partial \theta_\beta} \delta\theta_\alpha \delta\theta_\beta \quad (4.29)$$

In this approximation, the parameters which maximize the likelihood is directly solved as

$$\delta\theta_\alpha = - \sum_{\beta} \left(\frac{\partial^2 \ln \mathcal{L}}{\partial \theta_\alpha \partial \theta_\beta} \right)^{-1} \frac{\partial \ln \mathcal{L}}{\partial \theta_\beta}, \quad (4.30)$$

where first- and second-derivatives of the log likelihood function is explicitly calculated from equation (2.6), resulting in

$$\frac{\partial \ln \mathcal{L}}{\partial \theta_\alpha} = \frac{1}{2} \text{Tr} \left[\left(\mathbf{B} \mathbf{B}^T - C \right) (C^{-1} C_{,\alpha} C^{-1}) \right] \quad (4.31)$$

$$\begin{aligned} \frac{\partial^2 \ln \mathcal{L}}{\partial \theta_\alpha \partial \theta_\beta} = \frac{1}{2} \text{Tr} \left[\left(\mathbf{B} \mathbf{B}^T - C \right) (C^{-1} C_{,\alpha\beta} C^{-1} - C^{-1} C_{,\alpha} C^{-1} C_{,\beta} C^{-1} - C^{-1} C_{,\beta} C^{-1} C_{,\alpha} C^{-1}) \right. \\ \left. - C^{-1} C_{,\alpha} C^{-1} C_{,\beta} \right], \end{aligned} \quad (4.32)$$

where C is the correlation matrix and standard notations, $C_{,\alpha} = \partial C / \partial \theta_\alpha$, etc., are employed. Instead of intensive calculation of the curvature matrix of equation (4.32), the second-order derivatives are replaced by an expectation value, which is equivalent to the Fisher matrix:

$$F_{\alpha\beta} \equiv - \left\langle \frac{\partial^2 \ln \mathcal{L}}{\partial \theta_\alpha \partial \theta_\beta} \right\rangle = \frac{1}{2} \text{Tr} [C^{-1} C_{,\alpha} C^{-1} C_{,\beta}]. \quad (4.33)$$

In this way, we obtain the BJK's quadratic estimator,

$$\delta \theta_\alpha = \frac{1}{2} \sum_\beta (F^{-1})_{\alpha\beta} \text{Tr} \left[\left(\mathbf{B} \mathbf{B}^T - C \right) (C^{-1} C_{,\beta} C^{-1}) \right], \quad (4.34)$$

which proves to be very useful. Only few iterations are needed to reach the local maxima of the likelihood function when the band power of the CMB spectrum is estimated by this method (BJK). Since the projection matrix P of the projected correlation matrix $C = P R P^T$ of equation (2.5) is fixed throughout the likelihood maximization, the derivatives $C_{,\alpha}$ are straightforwardly calculated by numerically differentiating the correlation matrix R : $C_{,\alpha} = P R_{,\alpha} P^T$. For the cosmological parameters with polynomial influence on the correlation matrix, as considered in the section 4.1, the derivatives $C_{,\alpha}$ are obviously given without any numerical differentiation.

5. CONCLUSIONS AND DISCUSSION

Technical details of the methods in constructing the correlation matrix in redshift space, which are essential in direct likelihood analysis of the large-scale structure, have been presented. Making use of the most general analytic formula of the linear two-point correlation function in redshift space given by Matsubara (2000), a fast procedure to construct correlation matrices in redshift space has been explicitly provided. This procedure can be used for deep redshift surveys, as well as shallow surveys. The finger-of-God effects are not significant as long as the nonlinear modes are excluded by truncating the KL-modes. We have also given fast methods to produce correlation matrices in projected samples on the sky in which spatial and spherical curvature effects are taken into account. The Limber's equation is not appropriate for large separations. Some parameters polynomially depend on the correlation matrix. Those parameters are evidently simple to analyze. When the number of parameters are large, the quadratic estimator is a promising way to maximize the likelihood function.

The purpose of this paper is to describe technical details of computationally quick construction of correlation matrices. Parts of the present methods have been successfully applied to the real data, including the Las Campanas Redshift Survey and SDSS (Matsubara, Szalay & Landy 2000; Szalay et al. 2003; Pope et al. 2004). So far the application has been restricted to the shallow samples and the projected samples of galaxies. One of the final targets of the present methods is the application to the large-scale redshift surveys, which are deep and wide enough in redshift space. In this respect, our methods are effective in the analysis of the ongoing SDSS luminous red galaxy (LRG) sample (Eisenstein et al. 2001), in which $\sim 10^5$ galaxies are catalogued with redshift range of $z \sim 0.2$ – 0.5 over $\sim 10^4$ square degrees on the sky. Since this sample is dominated by the shot-noise on smaller scales, the KL transform is essential to maximally extract the cosmological information. The redshifts in the LRG sample are not very shallow as in the main galaxy sample, in which $z \lesssim 0.2$, the evolutionary effects on the clustering is detectable, and therefore geometry of the universe, nature of dark energy, etc., can be finely constrained because of the cosmological redshift-space distortion effects (Matsubara & Szalay 2001, 2002, 2003; Blake & Glazebrook 2003; Seo & Eisenstein 2003). In next-generation redshift surveys beyond the SDSS, the present methods will provide a unique technique in cosmological analyses of the survey data. In large and deep redshift surveys of the future, the linear regime will be more focused on, and the shot noise will be more severe than the present-day surveys. The advantage of the methods developed in this paper is much greater in those future surveys than the past shallow surveys.

We thank Daniel Eisenstein and Tamas Budavari for discussion. TM acknowledges support from the Ministry of Education, Culture, Sports, Science, and Technology, Grant-in-Aid for Encouragement of Young Scientists, 15740151, 2003. AS acknowledges support from grants NSF AST-9802 980 and NASA LTSA NAG-53503.

APPENDIX

CONSTRUCTION OF THE PROJECTION MATRIX BY THE KL EIGENMODES

In this appendix, the construction of the projection matrix P of equation (2.4) which reduces the dimensionality of the data space is reviewed, based on the method of Vogeley & Szalay (1996).

To capture maximum signals with minimum noise, one needs to keep the modes with the high S/N ratios and discard the modes with the low S/N ratios. For this purpose, we decompose the correlation matrix R into the signal part S plus the noise part N , $R = S + N$, assuming signals and noises are mutually uncorrelated. To normalize the noise correlations, we consider a linear transformation,

$$\mathbf{d}' = Q\mathbf{d}, \quad (\text{A1})$$

where Q is a non-degenerate $N \times N$ matrix, $\det Q \neq 0$, which is not necessarily a symmetric matrix. The transformation Q is chosen so that the noise correlation matrix in the new data vector \mathbf{d}' is transformed to an identity matrix:

$$N' = QNQ^T = I, \quad (\text{A2})$$

This transformation is referred to by *prewhitening* (Vogele & Szalay 1996).

However, the choice of the prewhitening matrix Q is not unique when the noise correlation matrix is not diagonal. For example, one can first diagonalize the noise correlation matrix N and then multiply a weighted diagonal matrix:

$$Q = Q_2 Q_1, \quad (\text{A3})$$

where Q_1 is an orthogonal matrix which diagonalize the noise matrix N :

$$Q_1 N Q_1^T = \text{diag}(\sigma_1^2, \sigma_2^2, \dots, \sigma_N^2), \quad (\text{A4})$$

and Q_2 is a diagonal matrix weighted by the inverse of the square root of the noise eigenvalues:

$$Q_2 = \text{diag}(\sigma_1^{-1}, \sigma_2^{-1}, \dots, \sigma_N^{-1}). \quad (\text{A5})$$

This choice is not the only possibility. Another example of the transformation Q is given by the Cholesky decomposition of the noise matrix, $N = LL^T$, where L is a lower triangular matrix. The choice $Q = L^{-1}$ also satisfies the equation (A2). Unless the noise matrix has diagonal form in first place, the matrix $Q_2 Q_1$ is not a triangular matrix and the matrix L^{-1} is a lower triangular matrix so that $Q_2 Q_1 \neq L^{-1}$ in general.

Once the noise matrix is normalized to an identity matrix by a certain choice of Q , the correlation matrix of equation (2.3) is transformed to

$$R' = QSQ^T + I. \quad (\text{A6})$$

Now, to obtain the *statistically orthogonal* set of data vectors, the prewhitened data is rotated so that the correlation matrix R' is diagonalized, solving the eigenvalue equation,

$$R'\Psi_n = \lambda'_n \Psi_n. \quad (\text{A7})$$

Since the diagonalization of the matrix R' keeps the noise term as the identity matrix, the noise contribution to an eigenvalue λ' is always unity. Therefore, the larger the eigenvalue is, the larger the signal-to-noise ratio of the corresponding eigenmode is. Sorting the eigenvalues in decreasing order,

$$\lambda'_1 \geq \lambda'_2 \geq \dots \geq \lambda'_M \geq \dots \geq \lambda'_N, \quad (\text{A8})$$

and discarding the modes with low eigenvalues of $\lambda'_{M+1}, \dots, \lambda'_N$, the natural choice of the projected data is

$$B_n = \Psi_n^T \mathbf{d}' = \Psi_n^T Q \mathbf{d} \quad (\text{A9})$$

where $n \leq M$, and the eigenvectors satisfy the orthonormality,

$$\Psi_n^T \Psi_m = \delta_{nm}. \quad (\text{A10})$$

Employing the projection matrix of the whitened data,

$$P' = (\Psi_1, \Psi_2, \dots, \Psi_M)^T, \quad (\text{A11})$$

the optimal projection matrix P is given by

$$P = P'Q \quad (\text{A12})$$

The eigenvalue λ'_n corresponds to “the signal-to-noise ratio plus unity” for each mode, since one can notice that the matrix Q is the “square root” of the noise matrix (c.f., eq.[A2]). Therefore, the quantities $\lambda_n \equiv \lambda'_n - 1$ correspond to the “signal-to-noise” eigenvalues. This is more clearly shown by the fact that the eigenvalue equation (A3) is equivalent to the generalized eigenvalue equation

$$S\Phi_n = \lambda_n N\Phi_n, \quad (\text{A13})$$

where $\Phi_n = Q^T \Psi_n$ is the signal-to-noise eigenmode, which is introduced by Bond (1995) in the analysis of the CMB data. The projection matrix P is simply given by

$$P = (\Phi_1, \Phi_2, \dots, \Phi_M)^T. \quad (\text{A14})$$

In this representation, it is explicitly seen that the choice of the projection matrix P is independent on the choice of the prewhitening matrix Q . The signal-to-noise eigenvectors Φ are no longer orthogonal, but are normalized by

$$\Phi_n^T N \Phi_m = \delta_{nm}. \quad (\text{A15})$$

A schematic explanation of obtaining the S/N eigenmodes is given in Figure C5. The solid ellipses represent the signal correlations and the dashed ellipses represent the noise correlations in two-dimensional data space. The S/N eigenmodes, or the KL modes, the directions of which is indicated by black arrows, determines the direction of the projection to reduce the dimension of the data space, retaining the maximal signals-to-noise ratio.

In the above procedure, the correlation matrix of the reduced data \mathbf{B} is a diagonal matrix since it is obtained by diagonalization of the correlation matrix of the prewhitened data \mathbf{d}' . Therefore, the reduced data is statistically orthogonal:

$$C_{nm} = \lambda'_n \delta_{nm} \quad (\text{A16})$$

where $\lambda'_n = \Psi_n^T R' \Psi_n = \Phi_n^T R \Phi_n = \lambda_n + 1 = \langle (B_n)^2 \rangle - \langle B_n \rangle^2$. The above orthogonality is achieved only when the true cosmological model of the correlation matrix R is known. In practice, the true parameters of the cosmological model are the object of study. Therefore the orthogonality of C_{nm} is only approximate and is never assumed in our likelihood analysis.

THE LINEAR FORMULA OF THE CORRELATION FUNCTION IN REDSHIFT SPACE WITH THE CURVATURE EFFECTS

In this appendix, we summarize the most general expression for the linear correlation function derived by Matsubara (2000). The high-redshift effects, the wide-angle effects, the peculiar velocity effects, and the selection effects are all included.

To describe the formula, we need the orthonormal modes of the Laplacian in the spatial section of the RW metric. That is, the orthonormal modes of the equation

$$(\Delta + k^2 - K)Z = 0, \quad (\text{B1})$$

prove to be useful. In the spatial section of the RW metric of equation (3.1), the above equation reduces to

$$\frac{1}{S_K^2(x)} \left[\frac{\partial}{\partial x} \left(S_K^2(x) \frac{\partial Z}{\partial x} \right) + \frac{1}{\sin \theta} \frac{\partial}{\partial \theta} \left(\sin \theta \frac{\partial Z}{\partial \theta} \right) + \frac{1}{\sin^2 \theta} \frac{\partial^2 Z}{\partial \phi^2} \right] + (k^2 - K)Z = 0. \quad (\text{B2})$$

Separating the variable Z into a radial part and an angular part, the orthonormal modes have the form $X_l(k, x)Y_l^m(\theta, \phi)$, where Y_l^m are the spherical harmonics. The orthonormality and the completeness of the spherical harmonics are useful:

$$\int \sin \theta d\theta d\phi Y_l^{m*}(\theta, \phi) Y_{l'}^{m'}(\theta, \phi) = \delta_{ll'} \delta_{mm'}, \quad (\text{B3})$$

$$\sum_{l=0}^{\infty} \sum_{m=-l}^l Y_l^{m*}(\theta, \phi) Y_l^m(\theta', \phi') = \frac{\delta(\theta - \theta') \delta(\phi - \phi')}{\sin \theta}. \quad (\text{B4})$$

The radial part X_l satisfies the differential equation

$$\frac{1}{S_K^2(x)} \frac{\partial}{\partial x} \left(S_K^2(x) \frac{\partial X_l}{\partial x} \right) + \left[k^2 - \frac{l(l+1)}{S_K^2(x)} \right] X_l = 0. \quad (\text{B5})$$

Putting $f = S_K^{1/2} X_l$ and $dz = S_K dx$, this equation reduces to the associated Legendre differential equation. The solutions of this equation are given by the conical function, the Bessel function, and the toroidal function, for negative, zero, and positive curvatures, respectively (Harrison 1967; Wilson 1983; Matsubara 2000). These solutions which are regular at the origin $x = 0$ are explicitly represented by

$$X_l(k, x) = \frac{S_K^l(x)}{\sqrt{N_l(k)}} \left(\frac{1}{S_K(x)} \frac{\partial}{\partial x} \right)^l \left(\frac{\sin kx}{S_K(x)} \right), \quad (\text{B6})$$

where

$$N_l(k) = \prod_{j=0}^l (k^2 - j^2 K) = k^2 (k^2 - K) (k^2 - 4K) \cdots (k^2 - l^2 K), \quad (\text{B7})$$

are the normalization constants. For $x \rightarrow 0$, X_l behaves like x^l with appropriate constants, and thus $X_l(k, 0) = \delta_{l0}$ (Harrison 1967). For the flat universe, $K = 0$, the equation (B6) is simply given by the spherical Bessel function, $X_l(k, x) = (-1)^l j_l(kx)$. For $K \leq 0$, k takes all positive values. In the case of positive curvature, $K > 0$, the 3-space is periodic and only discrete values $k = (l+1)\sqrt{K}, (l+2)\sqrt{K}, (l+3)\sqrt{K}, \dots$ are allowed. In the latter case, the functions (B6) are reduced to the Gegenbauer polynomials. The following recursion relations hold (Matsubara 2000):

$$\sqrt{k^2 - l^2 K} X_{l-1}(k, x) + (2l+1) \frac{C_K(x)}{S_K(x)} X_l(k, x) + \sqrt{k^2 - (l+1)^2 K} X_{l+1}(k, x) = 0 \quad (\text{B8})$$

The orthonormal and completeness relations are

$$4\pi \int_0^\infty dx S_K^2(x) X_l(k, x) X_l(k', x) = \frac{2\pi^2 \delta(k - k')}{k^2}, \quad (\text{B9})$$

$$\int_0^\infty \frac{k^2 dk}{2\pi^2} X_l(k, x) X_l(k, x') = \frac{\delta(x - x')}{4\pi S_K^2(x)}, \quad (\text{B10})$$

for $K \leq 0$, and

$$4\pi \int_0^\infty dx S_K^2(x) X_l(k_n, x) X_l(k_{n'}, x) = \frac{2\pi^2 \delta_{nn'}}{k_n^2}, \quad (\text{B11})$$

$$\frac{\sqrt{K}}{2\pi^2} \sum_{n=l+1}^\infty k_n^2 X_l(k_n, x) X_l(k_n, x') = \frac{\delta(x - x')}{4\pi S_K^2(x)}, \quad (\text{B12})$$

for $K > 0$, where $k_n \equiv n\sqrt{K}$. In the following, only the case of $K \leq 0$ is explicitly presented. The case of $K > 0$ is easily obtained by discretizing the variable $k \rightarrow k_n$ and by an interpretation of the integrals $\int_0^\infty dk \rightarrow \sqrt{K} \sum_{n=l+1}^\infty$, and

by $\delta(k - k') \rightarrow \delta_{nn'}$ etc. For our purpose, we need the explicit forms of X_l only up to $l = 4$:

$$X_0 = \frac{\sin kx}{kS_K(x)}, \quad (\text{B13})$$

$$X_1 = \frac{1}{\sqrt{N_1(k)} S_K^2(x)} [-C_K(x) \sin kx + kS_K(x) \cos kx], \quad (\text{B14})$$

$$X_2 = \frac{1}{\sqrt{N_2(k)} S_K^3(x)} \{ [3 - (k^2 + 2K)S_K^2(x)] \sin kx - 3kS_K(x)C_K(x) \cos kx \}, \quad (\text{B15})$$

$$X_3 = \frac{1}{\sqrt{N_3(k)} S_K^4(x)} \{ C_K(x) [-15 + 6(k^2 + K)S_K^2(x)] \sin kx \\ + kS_K(x) [15 - (k^2 + 11K)S_K^2(x)] \cos kx \}, \quad (\text{B16})$$

$$X_4 = \frac{1}{\sqrt{N_4(k)} S_K^5(x)} \{ [105 - 15(3k^2 + 8K)S_K^2(x) + (k^4 + 35Kk^2 + 24K^2)S_K^4(x)] \sin kx \\ - kS_K(x) [105 - 10(k^2 + 5K)S_K^2(x)] \cos kx \}, \quad (\text{B17})$$

where the function

$$C_K(x) \equiv \frac{dS_K(x)}{dx} = \begin{cases} \cosh(x\sqrt{-K}), & K < 0, \\ 1, & K = 0, \\ \cos(x\sqrt{K}), & K > 0, \end{cases} \quad (\text{B18})$$

has the properties

$$C_K^2(x) + KS_K^2(x) = 1, \quad (\text{B19})$$

$$\frac{dC_K(x)}{dx} = -KS_K(x). \quad (\text{B20})$$

Expanding the density contrast $\delta(x, \theta, \phi)$ in terms of the normal modes,

$$\delta(x, \theta, \phi) = \sum_{l=0}^{\infty} \sum_{m=-l}^l \int \frac{k^2 dk}{2\pi^2} \tilde{\delta}_{lm}(k) X_l(k, x) Y_l^m(\theta, \phi), \quad (\text{B21})$$

$$\tilde{\delta}_{lm}(k) = 4\pi \int dx S_K^2(x) \int \sin \theta d\theta d\phi \delta(x, \theta, \phi) X_l(k, x) Y_l^{m*}(\theta, \phi), \quad (\text{B22})$$

the power spectrum $P(k)$ is defined by

$$\langle \tilde{\delta}_{lm}^*(k) \tilde{\delta}_{l'm'}(k') \rangle = (2\pi)^3 \delta_{ll'} \delta_{mm'} \frac{\delta(k - k')}{k^2} P(k), \quad (\text{B23})$$

where only diagonal elements survive due to the statistical homogeneity and isotropy of the universe. The density contrast in redshift space is given by (Matsubara 2000)

$$\delta^{(s)}(x(z), \theta, \phi) = D(z) \left\{ b(z) + f(z) \left[\frac{\partial}{\partial x} + \alpha(z) \right] \frac{\partial}{\partial x} (\Delta + 3K)^{-1} \right\} \delta(x, \theta, \phi), \quad (\text{B24})$$

where $\delta(x, \theta, \phi)$ is the linear density contrast at the present time, $b(z)$ is the linear bias parameter at redshift z , $f(z)$ is the logarithmic derivative of the growth factor defined by equation (3.8). The linear operator $(\Delta + 3K)^{-1}$ denotes the Green's function of the operator $\Delta + 3K$, and

$$\alpha(z) = \frac{C_K[x(z)]}{S_K[x(z)]} \left\{ 2 + \frac{d \ln[D(z)f(z)\Phi(z)]}{d \ln S_K[x(z)]} \right\}, \quad (\text{B25})$$

where $\Phi(z)$ is the selection function per comoving volume. The selection function $\Phi(z)$ and the redshift distribution $n(z) = dN(< z)/dz$ of galaxies in the sample with a fixed sky area are related by $n(z)H(z) \propto \Phi(z)S_K^2(x(z))$. Therefore, the quantity $\alpha(z)$ is more conveniently expressed in terms of $n(z)$:

$$\alpha(z) = H(z) \frac{d}{dz} \ln[H(z)D(z)f(z)n(z)]. \quad (\text{B26})$$

In this equation, the term $Hd \ln(HDF)/dz$ has the order of the inverse of the Hubble scale, therefore is negligible, unless the clustering on Hubble scales is calculated. On the other hand, the term $Hd \ln n/dz$ is the order of inverse of the scale on which the distribution function $n(z)$ varies. When the correlation function on such a scale needs to be obtained, the factor α should be retained. Since the selection function $\Phi(z)$ usually is a decreasing function and the volume factor $S_K^2(x(z))$ is an increasing function, the distribution $n(z) = dN/dz$ does not significantly vary in the useful redshift range of a sample, unless galaxies near redshift edges are included. Therefore, if the redshift distribution $n(z)$ is approximately constant in

a sample, the factor α can be neglected. However, when the distribution dN/dz significantly varies in a sample, α must be kept in the analysis.

It is straightforward to obtain the Green's function since the density contrast is expanded by the eigenfunction of the Laplacian by equation (B21). The correlation function in redshift space is therefore given by $\xi^{(s)}(z_i, z_j, \theta_{ij}) = \langle \delta^{(s)}(x(z_i), \theta_i, \phi_i) \delta^{(s)}(x(z_j), \theta_j, \phi_j) \rangle$, where θ_{ij} is the angle between the two directions (θ_i, ϕ_i) and (θ_j, ϕ_j) . Defining the functions,

$$\xi_l^{(n)}(x) \equiv \frac{(-1)^n}{S_K^{2n-l}(x)} \int \frac{k^2 dk}{2\pi^2} \frac{\sqrt{N_l(k)}}{k(k^2 - 4K)^n} X_l(k, x) P(k), \quad (\text{B27})$$

we can explicitly represent the linear formula of the two-point correlation function in redshift space (Matsubara 2000):

$$\xi^{(s)}(z_i, z_j, \theta_{ij}) = b_i b_j D_i D_j \sum_{n=0}^2 \sum_{l=0}^{2n} c_l^{(n)}(x_i, x_j, \theta_{ij}) \xi_l^{(n)}(x_{ij}), \quad (\text{B28})$$

where we abbreviate $b_i = b(z_i)$, $D_i = D(z_i)$, $x_i = x(z_i)$ etc., $D(z)$ is the linear growth factor normalized by $D(z=0) = 1$, and $x(z)$ is the comoving distance given by equation (3.4). The quantity x_{ij} is the comoving separation of the two-points, which is obtained from x_i , x_j , and θ_{ij} by the geometric relation,

$$S_K^2(x_{ij}) = S_K^2(x_i) + S_K^2(x_j) - 2C_K(x_i)C_K(x_j)S_K(x_i)S_K(x_j)\cos\theta_{ij} - K S_K^2(x_i)S_K^2(x_j)(1 + \cos^2\theta_{ij}). \quad (\text{B29})$$

The coefficients $c_l^{(n)}$ are given by

$$c_0^{(0)} = 1 + \frac{1}{3}(\beta_i + \beta_j) + \frac{1}{15}\beta_i\beta_j \left(1 + 2\cos^2\tilde{\theta}_{ij}\right), \quad (\text{B30})$$

$$c_0^{(1)} = \left[\beta_i + \beta_j + \frac{2}{15}\beta_i\beta_j \left(4 + 3\cos\tilde{\theta}_{ij}\right)\right] |K| S_K^2(x_{ij}) - \frac{1}{3}\beta_i\beta_j A_{ij} A_{ji} \cos\tilde{\theta}_{ij}, \quad (\text{B31})$$

$$c_1^{(1)} = \beta_i A_{ij} \cos\gamma_{ij} + \beta_j A_{ji} \cos\gamma_{ji} + \frac{1}{5}\beta_i\beta_j \left[A_{ij} \left(\cos\gamma_{ij} - 2\cos\gamma_{ji} \cos\tilde{\theta}_{ij}\right) + A_{ji} \left(\cos\gamma_{ji} - 2\cos\gamma_{ij} \cos\tilde{\theta}_{ij}\right)\right], \quad (\text{B32})$$

$$c_2^{(1)} = \beta_i \left(\cos^2\gamma_{ij} - \frac{1}{3}\right) + \beta_j \left(\cos^2\gamma_{ji} - \frac{1}{3}\right) - \frac{1}{7}\beta_i\beta_j \left[\frac{2}{3} + \frac{4}{3}\cos^2\tilde{\theta}_{ij} - (\cos^2\gamma_{ij} + \cos^2\gamma_{ji}) + 4\cos\gamma_{ij} \cos\gamma_{ji} \cos\tilde{\theta}_{ij}\right], \quad (\text{B33})$$

$$c_0^{(2)} = \beta_i\beta_j \left(|K| S_K^2(x_{ij}) - A_{ij} A_{ji} |K| S_K^2(x_{ij})\right), \quad (\text{B34})$$

$$c_1^{(2)} = \beta_i\beta_j (A_{ij} \cos\gamma_{ij} + A_{ji} \cos\gamma_{ji}) |K| S_K^2(x_{ij}), \quad (\text{B35})$$

$$c_2^{(2)} = \frac{2}{7}\beta_i\beta_j \left[\cos^2\tilde{\theta}_{ij} - \frac{2}{3} + \frac{9}{2}(\cos^2\gamma_{ij} + \cos^2\gamma_{ji}) + 10\cos\gamma_{ij} \cos\gamma_{ji} \cos\tilde{\theta}_{ij}\right] |K| S_K^2(x_{ij}) + \beta_i\beta_j A_{ij} A_{ji} \left(\cos\gamma_{ij} \cos\gamma_{ji} + \frac{1}{3}\cos\tilde{\theta}_{ij}\right), \quad (\text{B36})$$

$$c_3^{(2)} = \frac{1}{5}\beta_i\beta_j \left[A_{ij} \left(5\cos\gamma_{ij} \cos^2\gamma_{ji} - \cos\gamma_{ij} + 2\cos\gamma_{ji} \cos\tilde{\theta}_{ij}\right) + A_{ji} \left(5\cos\gamma_{ji} \cos^2\gamma_{ij} - \cos\gamma_{ji} + 2\cos\gamma_{ij} \cos\tilde{\theta}_{ij}\right)\right], \quad (\text{B37})$$

$$c_4^{(2)} = \frac{1}{7}\beta_i\beta_j \left[\frac{1}{5} + \frac{2}{5}\cos^2\tilde{\theta}_{ij} - (\cos^2\gamma_{ij} + \cos^2\gamma_{ji}) + 4\cos\gamma_{ij} \cos\gamma_{ji} \cos\tilde{\theta}_{ij} + 7\cos^2\gamma_{ij} \cos^2\gamma_{ji}\right], \quad (\text{B38})$$

where the abbreviation $\beta_i = \beta(z_i)$ is employed and $\beta(z) = f(z)/b(z)$. The quantity A_{ij} is defined by

$$A_{ij} = S_K(x_{ij})\alpha(z_i). \quad (\text{B39})$$

The quantity A_{ji} is similarly defined with the replacement $i \leftrightarrow j$. The quantity γ_{ij} is an angle between the line of sight of x_i and the direction of the separation x_{ij} , which can be obtained by the equation

$$\cos\gamma_{ij} = \frac{S_K(x_i)C_K(x_j) - C_K(x_i)S_K(x_j)\cos\theta_{ij}}{S_K(x_{ij})}, \quad (\text{B40})$$

and γ_{ji} is similarly defined with the replacement $i \leftrightarrow j$. Finally, the quantity $\tilde{\theta}_{ij}$ is defined by

$$\cos\tilde{\theta}_{ij} = \frac{C_K(x_i)C_K(x_j)\cos\theta_{ij} + K S_K(x_i)S_K(x_j)}{C_K(x_i)C_K(x_j) + K S_K(x_i)S_K(x_j)\cos\theta_{ij}} = \frac{\sin\gamma_{ij}\sin\gamma_{ji}}{C_K(x_{ij})} - \cos\gamma_{ij}\cos\gamma_{ji}. \quad (\text{B41})$$

The matrix $\tilde{\theta}_{ij}$ is symmetric, while A_{ij} and γ_{ij} are not symmetric.

Although the expression of the two-point correlation function (B28) is somewhat tedious, the numerical calculation is straightforward. Especially, once the single-variable functions $f(z)$, $D(z)$, $x(z)$, $b(z)$, $\Phi(z)$, $\xi_t^{(n)}(x)$ are calculated and tabulated beforehand, then the evaluation of the correlation function does not require any further numerical integrations. This property is the essential part for the fast computation of the correlation matrix we have developed in this paper.

WINDOW FUNCTIONS AND THE EPANECHNIKOV KERNELS

In this appendix, window functions for a series of kernel functions, i.e., Epanechnikov kernels are explicitly given.

The Three-dimensional Case

First we consider the three-dimensional space. The window function is the 3-dimensional Fourier transform of the kernel function:

$$W(kR) = \int d^3x W_R(x) e^{-i\mathbf{k}\cdot\mathbf{x}} = 4\pi \int_0^\infty x^2 dx W_R(x) j_0(kx) \quad (C1)$$

There are two popular spherical kernels, i.e., the top-hat kernel,

$$W_R^{(T)}(x) = \frac{3}{4\pi R^3} \Theta(R-x), \quad W^{(T)}(kR) = \frac{3j_1(kR)}{kR}, \quad (C2)$$

where

$$\Theta(x) = \begin{cases} 1, & (x \geq 0), \\ 0, & (x < 0), \end{cases} \quad (C3)$$

is the Heaviside step function, and the Gaussian kernel,

$$W_R^{(G)}(x) = \frac{1}{(2\pi)^{3/2} R^3} e^{-x^2/(2R^2)}, \quad W^{(G)}(kR) = e^{-(kR)^2/2}. \quad (C4)$$

One of the advantages of the top-hat kernel is that it has finite support. It is a disadvantage that the Gaussian kernel extends to infinite volume, which should be truncated in actual analyses. However, the Gaussian kernel has an advantage that the window function $W^{(G)}(kR)$ drops off exponentially for large wavenumbers k , and thus the numerical integration with this factor is very stable. The function $W^{(T)}$ is an oscillating function and the envelope drops off as $(kR)^{-2}$, which converges much slower than the Gaussian window.

The slow drop-off of the Fourier transform of the top-hat kernel comes from the sharp discontinuity of the kernel at the edge, $x = R$. Accordingly, it is sometimes advantageous to use a kernel that is continuous at the edge, and at the same time, has finite support. One of such kernels is the Epanechnikov kernel,

$$W_R^{(E)}(x) = \frac{15}{8\pi R^3} \left(1 - \frac{x^2}{R^2}\right) \Theta(R-x), \quad W^{(E)}(kR) = \frac{15j_2(kR)}{(kR)^2}, \quad (C5)$$

which has a parabolic profile and the envelope of the Fourier transform drops off as $(kR)^{-3}$. While the Epanechnikov kernel is continuous on the edge, the radial derivative is not. The Epanechnikov kernel can be generalized such that the radial derivatives on the edge are also continuous. The generalized kernel is called m -weight Epanechnikov kernel, which is given by

$$W_R^{(Em)}(x) = \frac{(2m+3)!!}{2^{m+2} m! \pi R^3} \left(1 - \frac{x^2}{R^2}\right)^m \Theta(R-x), \quad W^{(Em)}(kR) = \frac{(2m+3)!! j_{m+1}(kR)}{(kR)^{m+1}}. \quad (C6)$$

The original Epanechnikov kernel is the 1-weight kernel, $W_R^{(E1)}$. Top-hat kernel is also from this sequence with $m = 0$. The m -weight Epanechnikov kernel is continuous up to $(m-1)$ derivatives on the edge. The envelope of the Fourier transform drops off as $(kR)^{-m-2}$, so that the convergence is faster for higher orders. The effective width of the kernel is smaller than R , especially for higher weights m . In this respect, the size of the kernels is more conveniently represented by the ‘‘variance’’ of the kernels,

$$\mathcal{R} \equiv \left[\int d^3x W_R^{(Em)}(x) x^2 \right]^{1/2} = \left(\frac{3}{2m+5} \right)^{1/2} R. \quad (C7)$$

For the top-hat kernel, the smoothing radius R_T corresponds to $R_T = (5/3)^{1/2} \mathcal{R}$. In the limit $m \rightarrow \infty$, with \mathcal{R} fixed, the m -weight Epanechnikov kernel reduces to the Gaussian kernel. In fact,

$$W_R^{(Em)}(x) \xrightarrow[\mathcal{R} \text{ fixed}]{m \rightarrow \infty} W_{R_G}^{(G)}(x), \quad (C8)$$

where the Gaussian smoothing length R_G corresponds to $R_G = \mathcal{R}/\sqrt{3}$. Therefore, the generalized Epanechnikov kernels contain both the top-hat kernel and the Gaussian kernels at $m = 0$ and $m = \infty$, respectively.

The Two-dimensional Case

Next we summarize the case for the two-dimensional space. The window function is given by

$$W(l\theta_s) = \int d^2\theta W_{\theta_s}(\theta) e^{-i\mathbf{l}\cdot\boldsymbol{\theta}} = 2\pi \int_0^\infty \theta d\theta W_{\theta_s}(\theta) J_0(l\theta). \quad (C9)$$

The top-hat kernel and its window function are

$$W_{\theta_s}^{(T)}(\theta) = \frac{1}{\pi\theta_s^2} \Theta(\theta_s - \theta), \quad W^{(T)}(l\theta_s) = \frac{2J_1(l\theta_s)}{l\theta_s}, \quad (C10)$$

and Gaussian counterparts are

$$W_{\theta_s}^{(G)}(\theta) = \frac{1}{2\pi\theta_s^2} e^{-\theta^2/(2\theta_s^2)}, \quad W^{(G)}(l\theta_s) = e^{-l^2\theta_s^2/2}. \quad (C11)$$

The Epanechnikov kernel in 2-dimension is given by

$$W_{\theta_s}^{(E)}(\theta) = \frac{2}{\pi\theta_s^2} \left(1 - \frac{\theta^2}{\theta_s^2}\right) \Theta(\theta_s - \theta), \quad W^{(E)}(l\theta_s) = \frac{8J_2(l\theta_s)}{(l\theta_s)^2}. \quad (C12)$$

which has a parabolic profile and the envelope of the Fourier transform drops off as $(l\theta_s)^{-5/2}$. The m -weight Epanechnikov kernel is derived as

$$W_{\theta_s}^{(Em)}(\theta) = \frac{m+1}{\pi\theta_s^2} \left(1 - \frac{\theta^2}{\theta_s^2}\right)^m \Theta(\theta_s - \theta), \quad W^{(Em)}(l\theta_s) = \frac{2^{m+1}(m+1)!J_{m+1}(l\theta_s)}{(l\theta_s)^{m+1}}. \quad (C13)$$

The envelope of the Fourier transform drops off as $(kR)^{-m-3/2}$, so that the convergence is faster for higher weights. The effective width of the kernel is smaller than R , especially for higher weights m . The size of the kernels is alternatively represented by the “variance” of the kernels,

$$\vartheta_s \equiv \left[\int d^2\theta W_{\theta_s}^{(Em)}(\theta) \theta^2 \right]^{1/2} = \frac{\theta_s}{\sqrt{m+2}} \quad (C14)$$

For the top-hat kernel, the smoothing radius θ_T corresponds to $\theta_T = \sqrt{2}\vartheta_s$. In the limit $m \rightarrow \infty$, with ϑ_s fixed, the m -weight Epanechnikov kernel reduces to the Gaussian kernel. In fact,

$$W_{\theta_s}^{(Em)}(\theta) \xrightarrow[m_s \text{ fixed}]{m \rightarrow \infty} W_{\theta_G}^{(G)}(x), \quad (C15)$$

where the Gaussian smoothing length θ_G corresponds to $\theta_G = \vartheta_s/\sqrt{2}$.

REFERENCES

- Alcock, C. & Paczyński, B. 1979, *Nature*, 281, 358
 Arfken, G. B. & Weber, H. J. 2001, *Mathematical Methods for Physicists*, Fifth Edition (San Diego; Harcourt/Academic Press)
 Ballinger, W. E. & Peacock, J. A. & Heavens, A. F. 1996, *MNRAS*, 282, 877
 Bennett, C. L. et al. 2003, *ApJS*, 148, 1
 Blake, C. & Glazebrook, K. 2003, *ApJ*, 594, 665
 Bond, J. R. 1995, *Physical Review Letters*, 74, 4369
 Bond, J. R., Jaffe, A. H., & Knox, L. 1998, *Phys. Rev. D*, 57, 2117
 Cole, S., Fisher, K. B., & Weinberg, D. H. 1995, *MNRAS*, 275, 515
 Colless, M. et al. 2001, *MNRAS*, 328, 1039
 Davis, M. & Peebles, P. J. E. 1983, *ApJ*, 267, 465
 Davis, M. et al. 2003, *Proc. SPIE*, 4834, 161
 Efstathiou, G. & Moody, S. J. 2001, *MNRAS*, 325, 1603
 Eisenstein, D. J. & Hu, W. 1998, *ApJ*, 496, 605
 Eisenstein, D. J. et al. 2001, *AJ*, 122, 2267
 Feldman, H. A., Kaiser, N., & Peacock, J. A. 1994, *ApJ*, 426, 23
 Hamilton, A. J. S. 1992, *ApJ*, 385, L5
 Hamilton, A. J. S. 1997, *MNRAS*, 289, 295
 Hamilton, A. J. S. & Tegmark, M. 2000, *MNRAS*, 312, 285
 Hamilton, A. J. S., Tegmark, M., & Padmanabhan, N. 2000, *MNRAS*, 317, L23
 Harrison, E. R. 1967, *Rev. Mod. Phys.*, 39, 862
 Huterer, D., Knox, L., & Nichol, R. C. 2001, *ApJ*, 555, 547
 Kaiser, N. 1987, *MNRAS*, 227, 1
 Matsubara, T. 2000, *ApJ*, 535, 1
 Matsubara, T. & Suto, Y. 1996, *ApJ*, 470, L1
 Matsubara, T., Szalay, A. S., & Landy, S. D. 2000, *ApJ*, 535, L1
 Matsubara, T. & Szalay, A. S. 2001, *ApJ*, 556, L67
 Matsubara, T. & Szalay, A. S. 2002, *ApJ*, 574, 1
 Matsubara, T. & Szalay, A. S. 2003, *Phys. Rev. Lett.*, 90, 021302
 Park, C., Vogeley, M. S., Geller, M. J., & Huchra, J. P. 1994, *ApJ*, 431, 569
 Peacock, J. A. 1992, *New Insights into the Universe*, Proceedings of a Summer School Held in Valencia, Spain, 23-27 September 1991. Edited by V. J. Martinez, M. Portilla, and D. Saez. Springer-Verlag Berlin Heidelberg New York. Also Lecture Notes in Physics, volume 408, 1992, p.1, 1
 Peacock, J. A. & Dodds, S. J. 1994, *MNRAS*, 267, 1020
 Peebles, P. J. E. 1980, *The Large-Scale Structure of the Universe* (Princeton; Princeton University Press)
 Pope, A. et al., *ApJL*, submitted.
 Press, W. H., Teukolsky, S. A., Vetterling, W. T., & Flannery, B. P. 1992, *Numerical Recipes in FORTRAN* (2d ed.; Cambridge: Cambridge Univ. Press)
 Ratna, B. & Peebles, P. J. E. 1995, *Phys. Rev. D*, 52, 1837
 Schuecker, P., Guzzo, L., Collins, C. A., & Böhringer, H. 2002, *MNRAS*, 335, 807
 Scoccimarro, R. & Frieman, J. 1996, *ApJS*, 105, 37
 Seo, H. & Eisenstein, D. J. 2003, *arXiv:astro-ph/0307460*
 Spergel, D. N. et al. 2003, *ApJS*, 148, 175
 Szalay, A. S., Matsubara, T., & Landy, S. D. 1998, *ApJ*, 498, L1
 Szalay, A. S. et al. 2003, *ApJ*, 591, 1
 Taylor, A. N., Ballinger, W. E., Heavens, A. F., & Tadros, H. 2001, *MNRAS*, 327, 689
 Tegmark, M., Hamilton, A. J. S., Strauss, M. A., Vogeley, M. S., & Szalay, A. S. 1998, *ApJ*, 499, 555
 Tegmark, M., Taylor, A. N., & Heavens, A. F. 1997, *ApJ*, 480, 22
 Tegmark, M., Hamilton, A. J. S., & Xu, Y. 2002, *MNRAS*, 335, 887
 Tegmark, M. et al. 2003, *arXiv:astro-ph/0310725*
 Vogeley, M. S. & Szalay, A. S. 1996, *ApJ*, 465, 34
 Wilson, M. L. 1983, *ApJ*, 273, 2
 York, D. G. et al. 2000, *AJ*, 120, 1579

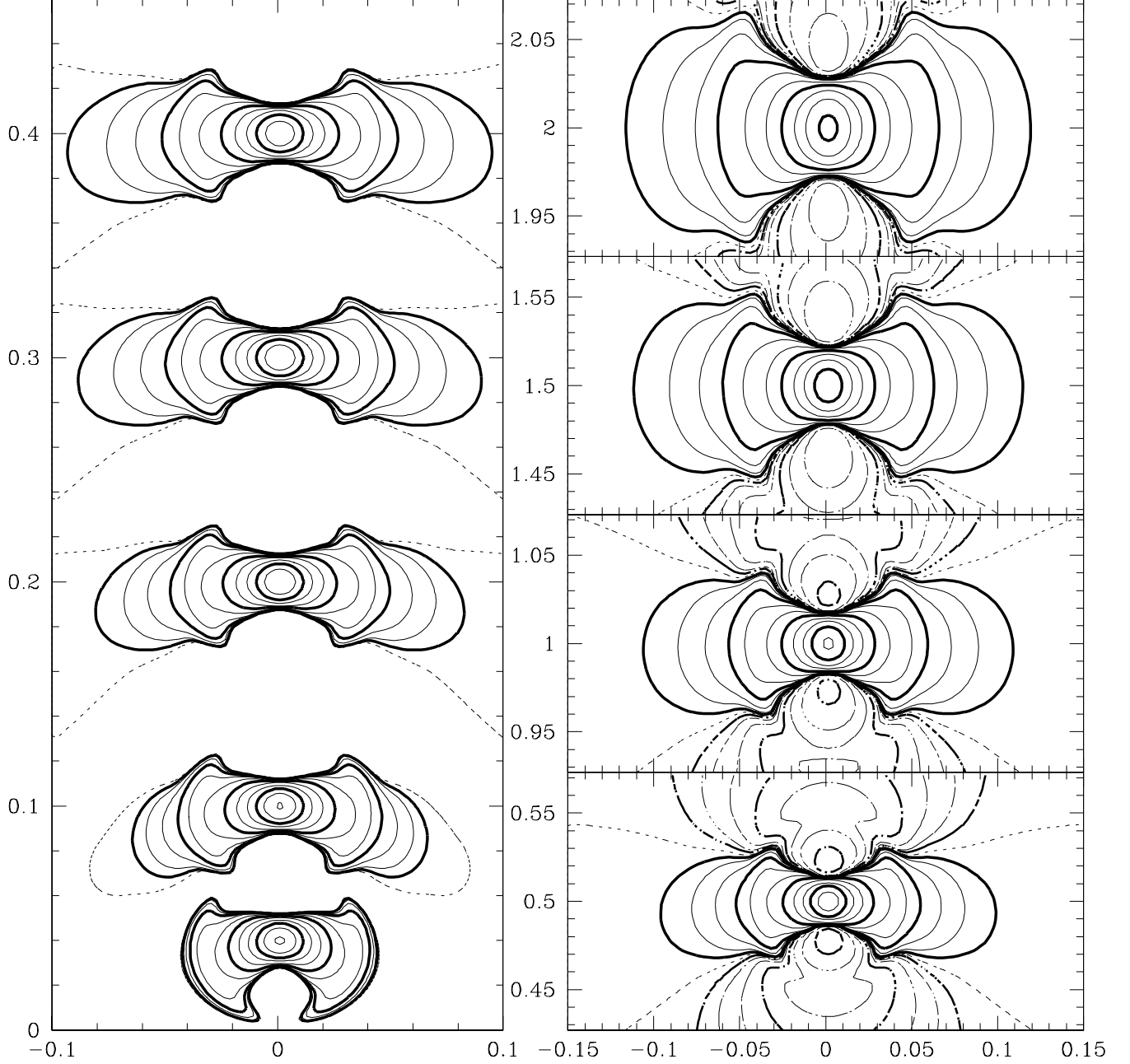


FIG. C1.— The smoothed ($R = 15 h^{-1} \text{Mpc}$) correlation function in redshift space in the concordance model: $\Omega_{M0} = 0.3$, $\Omega_{K0} = 0$, $w = -1$, $h = 0.7$, $f_{\text{baryon}} = 0.15$, $b = 1$, $\sigma_8 = 1$. Contour lines indicate the value of the smoothed correlation function around the centers at redshifts $z_i = 0.04, 0.1, 0.2, 0.3, 0.4, 0.5, 1, 1.5, 2$. The coordinate axes correspond to $(z_j \sin \theta_{ij}, z_j \cos \theta_{ij})$, i.e., the direct z -space. The contours have the intervals of $\Delta \log_{10} \xi_{ij} = 1/3$. Thick contours indicate $\xi_{ij} = 0.1, 0.01, 10^{-3}, 10^{-4}$ from inner to outer contours, respectively. The zero-points of ξ_{ij} are plotted by dotted lines. In the right panels, negative regions are also shown by dashed contours with the same contour levels with minus signs.

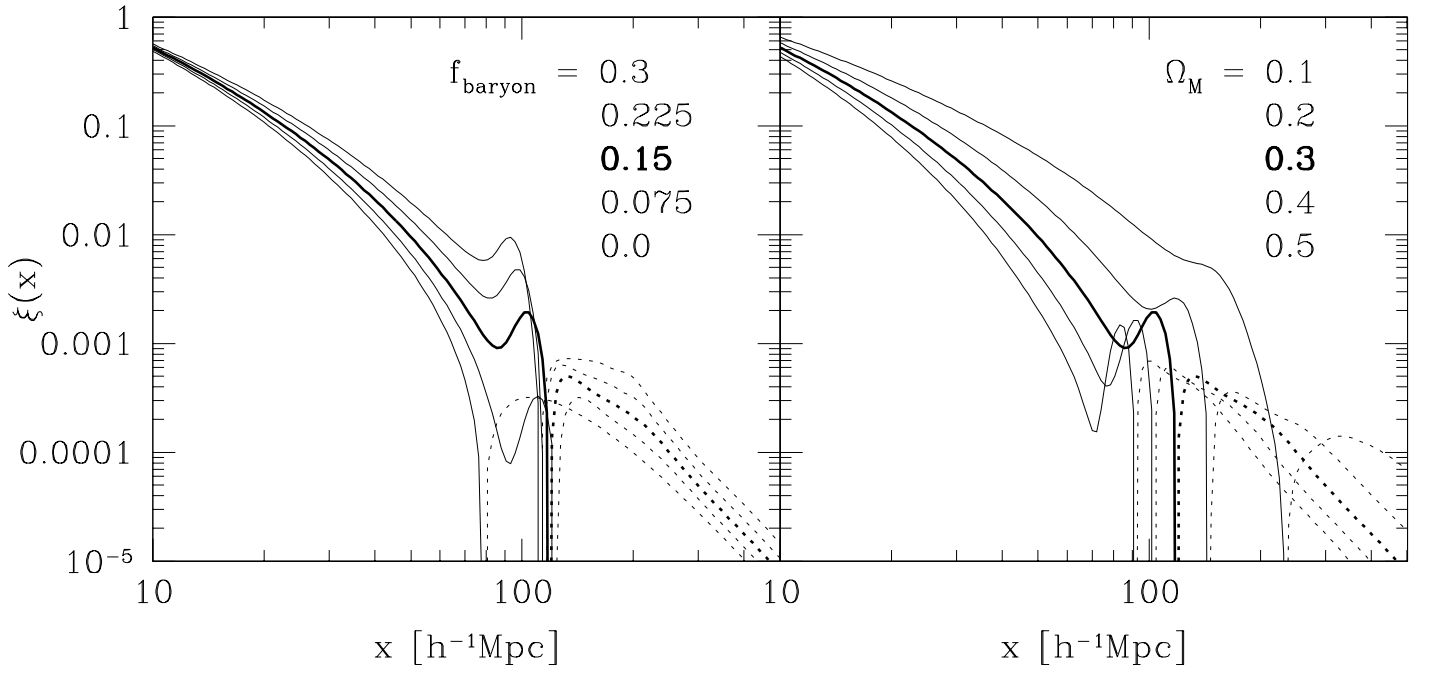


FIG. C2.— The correlation function in real space, $\xi(x)$. The thick lines correspond to the concordance model which is the same as in the Figure C1. The baryon fraction f_{baryon} is varied in the left panel, and the total density parameter Ω_{M0} is varied in the right panel, as indicated in the figures. Higher baryon fraction and lower density parameter both give higher amplitudes of the correlations. Dotted lines indicate the negative correlations.

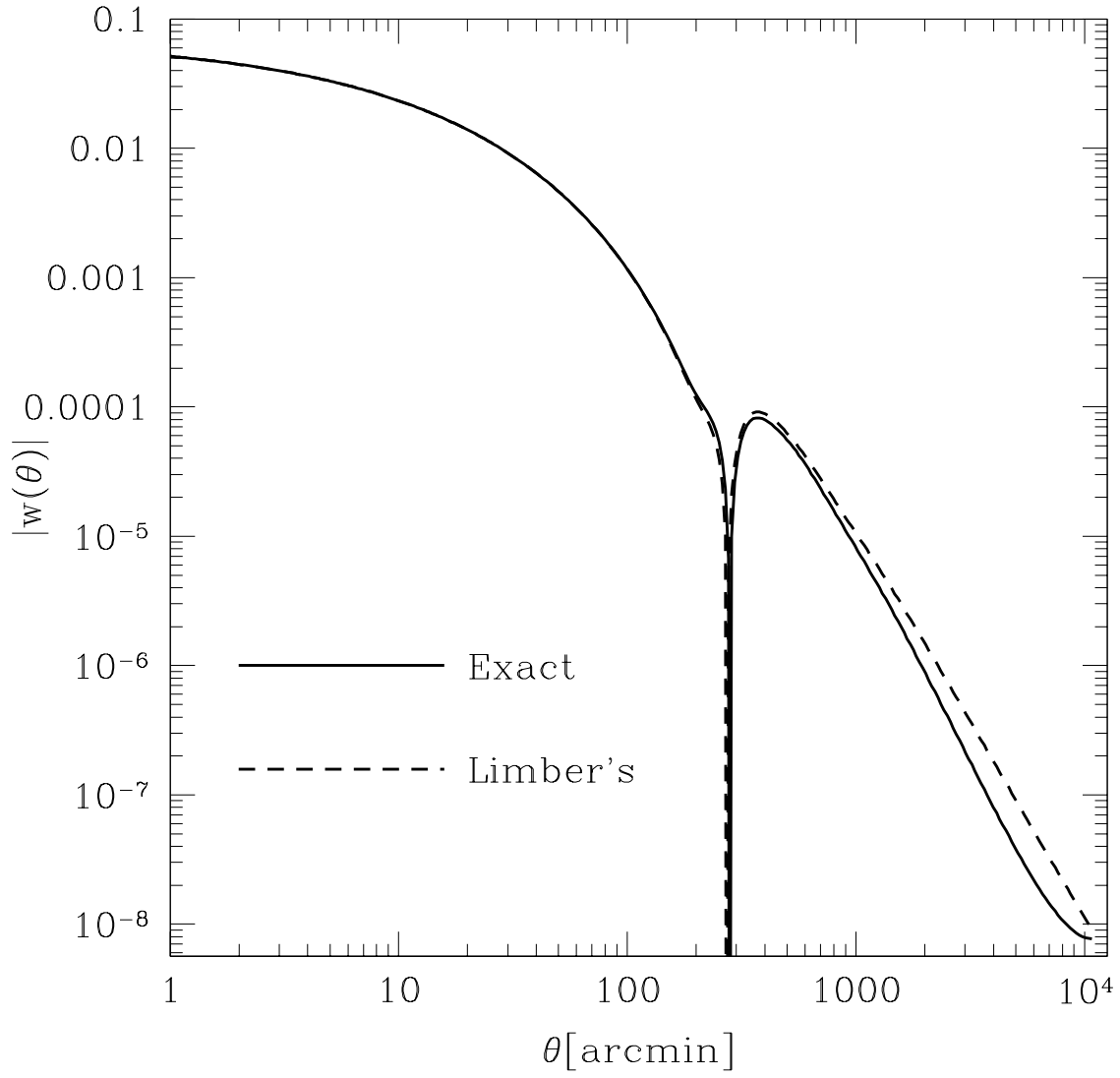


FIG. C3.— Angular correlation function for the concordance model. The solid line shows the exact prediction of the linear theory (see text). The dashed line shows the prediction from Limber's equation.

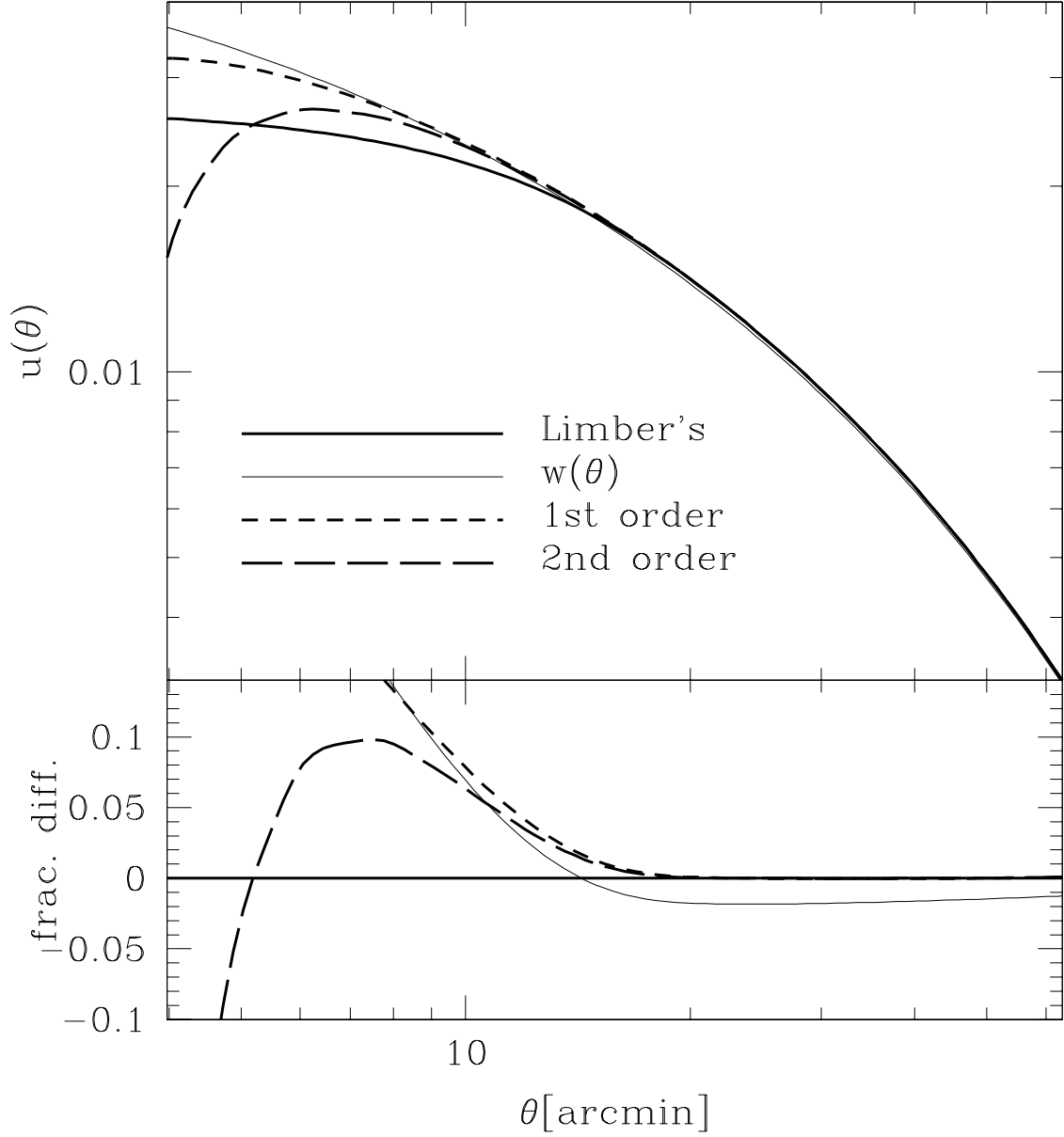


FIG. C4.— The smoothed angular correlation function $u(\theta)$ around the smoothing scale ($\theta_s = 10$ arcmin.). Thin solid line: the bare angular correlations. Thick solid line: smoothed correlations with Limber's equation. Short-dashed line: Taylor approximation up to 1st order. Long-dashed line: Taylor approximation up to 2nd order. The lower panel shows the fractional differences with respect to the prediction of Limber's equation, which gives the precise value of $u(\theta)$ in the angle range here.

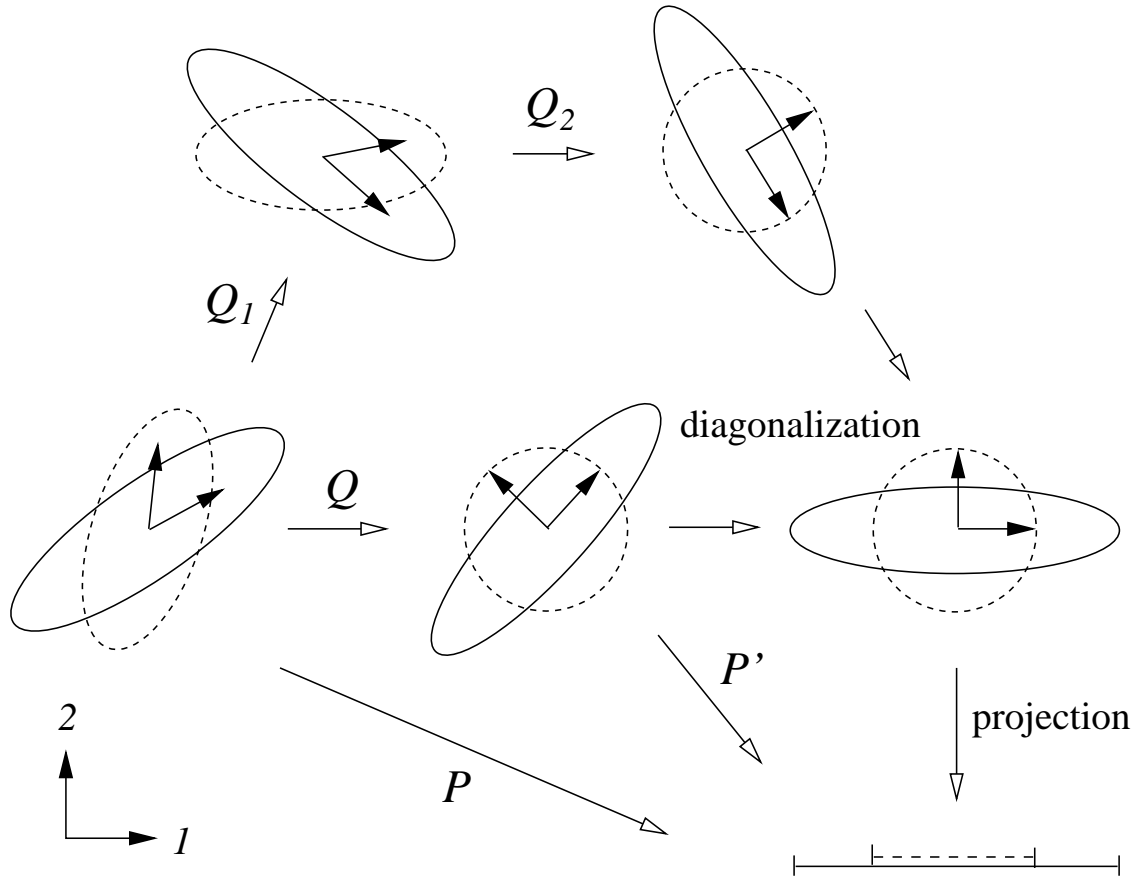


FIG. C5.— A schematic explanation of the projection by the S/N eigenmodes, or KL eigenmodes. Solid ellipses represent the signal correlations and dashed ellipses represent the noise correlations in two-dimensional data space. The directions of the S/N eigenmodes are indicated by black arrows. The matrix Q_1 diagonalizes the noise correlations, and Q_2 rescales the data space to obtain the prewhitened noise matrix. Although there is not a unique way to choose a prewhitening matrix Q , the resulting projection matrix P is independent of the choice. The generalized eigenvalue equation directly gives the projection matrix P . The original data space is projected onto the reduced data space, retaining only modes with the highest S/N ratio.